

Finite Volume Evolution Galerkin Methods for Nonlinear Hyperbolic Systems

M. Lukáčová-Medvid'ová,^{*,†} J. Saibertová,[†] and G. Warnecke^{*}

^{*}*Institute of Analysis and Numerics, Otto-von-Guericke-Universität Magdeburg, Universitätsplatz 2, 39 106 Magdeburg, Germany; and* [†]*Department of Mathematics, Faculty of Mechanical Engineering, University of Technology Brno, Technická 2, 616 39 Brno, Czech Republic*
E-mail: Lukacova@fme.vutbr.cz, Saibertova@mat.fme.vutbr.cz, and
Gerald.Warnecke@mathematik.uni-magdeburg.de

Received January 31, 2002; revised July 23, 2002; accepted September 18, 2002

We present new truly multidimensional schemes of higher order within the framework of finite volume evolution Galerkin (FVEG) methods for systems of nonlinear hyperbolic conservation laws. These methods couple a finite volume formulation with approximate evolution operators. The latter are constructed using the bicharacteristics of the multidimensional hyperbolic system, such that all of the infinitely many directions of wave propagation are taken into account. Following our previous results for the wave equation system, we derive approximate evolution operators for the linearized Euler equations. The integrals along the Mach cone and along the cell interfaces are evaluated exactly, as well as by means of numerical quadratures. The influence of these numerical quadratures will be discussed. Second-order resolution is obtained using a conservative piecewise bilinear recovery and the midpoint rule approximation for time integration. We prove error estimates for the finite volume evolution Galerkin scheme for linear systems with constant coefficients. Several numerical experiments for the nonlinear Euler equations, which confirm the accuracy and good multidimensional behavior of the FVEG schemes, are presented as well. © 2002 Elsevier Science (USA)

Key Words: genuinely multidimensional schemes; hyperbolic systems; wave equation; Euler equations; evolution Galerkin schemes.

1. INTRODUCTION

In recent years the most commonly used methods for hyperbolic problems were finite volume methods which were based on a quasidimensional splitting using one-dimensional Riemann solvers. These were applied in directions determined by the grid instead of the flow. This can yield spurious local wave structures. Actually, it turned out that in certain cases, e.g.,

when waves are propagating in directions that are oblique with respect to a rectangular mesh, this approach leads to structural deficiencies and large errors in the solution. Therefore, our emphasis has been placed on developing genuinely multidimensional methods.

The first criticism of using one-dimensional Riemann solvers was given by Roe [30]. Further description of several failings of one-dimensional Riemann solvers applied to multidimensional Euler equations can be found in Quirk [29]. In particular such phenomena as the “odd-even-decoupling” and “carbuncle” problem are reported therein.

In the 1990s Deconinck *et al.* [7] presented the fluctuation splitting schemes. The propagation information is decomposed into a discrete number of simple waves. These are then distributed in flow direction to the cell vertices. In 1997 Le Veque presented the wave propagation algorithm for multidimensional systems of conservation laws [13]. The scheme still works with a one-dimensional Riemann solver; however, it not only approximates the fluxes in x and y directions normal to cell interfaces, it also considers the tangential fluxes. During the same time Fey developed the method of transport (MoT) for the Euler equations [9]. Fey’s method is based on decomposing the Euler equations into a finite number of advection equations and solving each of them separately using a multidimensional scheme. The MoT suffers from an inconsistency at sonic points when used with piecewise constant recovery. Recently, Noelle introduced in [27] a simplified version of the MoT scheme using the so-called interface-centered evolution. Noelle’s method is consistent at all points, including sonic points.

Other multidimensional approaches include Colella’s corner transport upwind (CTU) [6], the weighted-average-flux (WAF) scheme of Billet and Toro [2], and the method of Brio *et al.* [3]. The latter is based on the use of the so-called multistate linear Riemann solver, which corrects, in a multidimensional manner, contributions from corners of the computational cells. The explicit solution of the linear multistate Riemann problem is based on the use of the Kirchhoff formulae for linear second-order wave equations (see also [10] for related work).

In our work we use, similarly to Brio *et al.*, linear solvers to take into account the multidimensional nature of hyperbolic systems. The main advantages of this approach are improved resolution properties and the directional unsplit nature of the scheme. On the other hand, we work with a general theory of bicharacteristics for linear hyperbolic systems of first order in order to obtain the so-called approximate evolution operators. Thus, our approach is more general and can be extended to systems that are not easily reduced to the wave equation (see Li *et al.* [14]).

The basic idea of the *evolution Galerkin schemes* (EG), introduced by Morton and co-workers (see, e.g., [15, 25]), is the following. Transport quantities are shifted along characteristics and then projected onto a finite element space. Thus, these methods connect the theory of characteristics for hyperbolic problems with finite element ideas. For scalar equations a complete theory and error analysis are available. An application to the one-dimensional Euler equations was described by Childs [5].

It was Ostkamp [28] who first generalized EG schemes to multidimensional systems. In [17] we improved the stability as well as accuracy of Ostkamp’s original finite difference scheme. In [23] we derived new second-order finite difference EG schemes. Higher order *finite volume evolution Galerkin* (FVEG) schemes were studied for linear wave equation systems in [18, 19]. The aim of this contribution is to derive and analyze new multidimensional high-resolution FVEG methods for systems of *nonlinear* hyperbolic conservation laws (see also [21] for a related paper).

In order to construct a genuinely multidimensional scheme the exact integral equations are derived from a general theory of bicharacteristics for linear (or linearized) hyperbolic systems. These are further approximated by an approximate evolution operator in such a way that all of the infinitely many directions of propagation of bicharacteristics are explicitly taken into account. In the finite volume framework the approximate evolution operator is then used to evolve the solution along cell interfaces in order to compute fluxes on edges. This step can be considered a predictor step. In a corrector step the finite volume update is then made.

The finite volume evolution Galerkin methods are a genuine generalization of the original idea of Godunov using an evolution operator for a system in more than one space dimension. They combine the usually conflicting design objectives of using the conservation form and following the characteristics, or bicharacteristics. Instead of solving one-dimensional Riemann problems in normal directions to cell interfaces by some approximate Riemann solvers, we compute fluxes in a more multidimensional manner. This is the novel feature of our method.

This paper is organized as follows. In Section 2 approximate evolution operators for the linearized Euler equations are derived. We follow the lines of our recent results [17] for the linear wave equation system. The formulation of the second-order finite volume evolution Galerkin scheme is given in Section 3. Second-order resolution is obtained with a conservative bilinear recovery in space and the midpoint rule approximation in time. In order to suppress oscillations of the solution at discontinuities several techniques of limiting are discussed. We illustrate the use of the method for the nonlinear system of Euler equations and present details concerning the linearization used. In Section 4 the error analysis of the FVEG schemes is presented. First we study the linearization error which is due to the approximation of a nonlinear hyperbolic system of first order by a linearized one. Linearization is done by freezing the Jacobian matrices at a suitable state. Further, the global numerical error for the case of linear or linearized systems is studied. We prove that the error in space as well as in time is of second order. Numerical results, which confirm higher order accuracy as well as good multidimensional resolution of the FVEG schemes, are shown in Section 5. We present results for the so-called Sod 2D problem and two-dimensional Riemann problems (see, e.g., [31]). Our numerical experiments demonstrate that the FVEG methods satisfy the entropy condition also at sonic rarefaction waves and no entropy fix is needed.

2. APPROXIMATE EVOLUTION OPERATORS: THE LINEARIZED EULER EQUATIONS

The key ingredient in our genuinely multidimensional schemes are approximate evolution operators that are derived from an integral equation. The integral equation is obtained using integration along bicharacteristics of the system. From this integral equation one can develop a number of approximate evolution operators.

The basic approach for general linear systems with constant coefficients and its application to a 3×3 system for the two-dimensional wave equation were presented in [17]. Here we give details for the case of the 4×4 system of the linearized Euler equations with frozen coefficients. It describes not only the propagation of acoustic waves, it also allows advective terms as additional difficulty.

2.1. The Linearized Euler Equations and Their Exact Integral Equation

In order to derive the integral equations for nonlinear hyperbolic systems a suitable linearization and freezing of coefficients has to be imposed first. This is achieved by freezing the Jacobian matrices at a suitable point. In this section we derive the integral equations for such linearized systems. In Section 3.2 we will specify the linearization and in Section 4.1 we will analyze the error introduced by the linearization.

We will illustrate the whole procedure for the Euler equations of gas dynamics and start with the system written in primitive variables,

$$\mathbf{v}_t + \mathbf{A}_1(\mathbf{v})\mathbf{v}_x + \mathbf{A}_2(\mathbf{v})\mathbf{v}_y = 0, \quad \mathbf{x} = (x, y)^T \in \mathbb{R}^2, \quad (2.1)$$

where

$$\mathbf{v} := \begin{pmatrix} \rho \\ u \\ v \\ p \end{pmatrix}, \quad \mathbf{A}_1 := \begin{pmatrix} u & \rho & 0 & 0 \\ 0 & u & 0 & \frac{1}{\rho} \\ 0 & 0 & u & 0 \\ 0 & \gamma p & 0 & u \end{pmatrix}, \quad \mathbf{A}_2 := \begin{pmatrix} v & 0 & \rho & 0 \\ 0 & v & 0 & 0 \\ 0 & 0 & v & \frac{1}{\rho} \\ 0 & 0 & \gamma p & v \end{pmatrix}.$$

This is the simplest and most convenient form for studying the bicharacteristics of the system away from discontinuities, i.e., shocks and contacts. Here ρ denotes the density, u and v are the components of velocities, p is the pressure, and γ is the isentropic exponent. We consider $\gamma = 1.4$ for dry air. To derive the integral equations we linearize system (2.1) by freezing the Jacobian matrices at a point $\tilde{P} = (\tilde{x}, \tilde{y}, \tilde{t})$. Denote by $\tilde{\mathbf{v}} = (\tilde{\rho}, \tilde{u}, \tilde{v}, \tilde{p})$ the local variables at point \tilde{P} and by \tilde{a} the local speed of sound there; i.e. $\tilde{a} = \sqrt{\frac{\gamma \tilde{p}}{\tilde{\rho}}}$. Thus, the linearized system (2.1) with frozen constant coefficients has the form

$$\mathbf{v}_t + \mathbf{A}_1(\tilde{\mathbf{v}})\mathbf{v}_x + \mathbf{A}_2(\tilde{\mathbf{v}})\mathbf{v}_y = 0, \quad \mathbf{x} = (x, y)^T \in \mathbb{R}^2. \quad (2.2)$$

The eigenvalues of the matrix pencil $\mathbf{A}(\tilde{\mathbf{v}}) = \mathbf{A}_1(\tilde{\mathbf{v}})n_x + \mathbf{A}_2(\tilde{\mathbf{v}})n_y$, where $\mathbf{n} = \mathbf{n}(\theta) = (n_x, n_y)^T = (\cos \theta, \sin \theta)^T \in \mathbb{R}^2$, are

$$\lambda_1 = \tilde{u} \cos \theta + \tilde{v} \sin \theta - \tilde{a},$$

$$\lambda_2 = \lambda_3 = \tilde{u} \cos \theta + \tilde{v} \sin \theta,$$

$$\lambda_4 = \tilde{u} \cos \theta + \tilde{v} \sin \theta + \tilde{a},$$

and the corresponding linearly independent right eigenvectors are

$$\mathbf{r}_1 = \begin{pmatrix} -\frac{\tilde{p}}{\tilde{a}} \\ \cos \theta \\ \sin \theta \\ -\tilde{\rho} \tilde{a} \end{pmatrix}, \quad \mathbf{r}_2 = \begin{pmatrix} 1 \\ 0 \\ 0 \\ 0 \end{pmatrix}, \quad \mathbf{r}_3 = \begin{pmatrix} 0 \\ \sin \theta \\ -\cos \theta \\ 0 \end{pmatrix}, \quad \mathbf{r}_4 = \begin{pmatrix} \frac{\tilde{p}}{\tilde{a}} \\ \cos \theta \\ \sin \theta \\ \tilde{\rho} \tilde{a} \end{pmatrix}.$$

Let $\mathbf{R}(\tilde{\mathbf{v}})$ be the matrix of the right eigenvectors. The inverse of $\mathbf{R}(\tilde{\mathbf{v}})$ is

$$\mathbf{R}^{-1}(\tilde{\mathbf{v}}) = \frac{1}{2} \begin{pmatrix} 0 & \cos \theta & \sin \theta & -1/(2\tilde{\rho}\tilde{a}) \\ 1 & 0 & 0 & -1/\tilde{a}^2 \\ 0 & \sin \theta & -\cos \theta & 0 \\ 0 & \cos \theta & \sin \theta & 1/(2\tilde{\rho}\tilde{a}) \end{pmatrix}.$$

Multiplying system (2.2) by $\mathbf{R}^{-1}(\tilde{\mathbf{v}})$ from the left we obtain the characteristic system

$$\mathbf{w}_t + \mathbf{B}_1(\tilde{\mathbf{v}})\mathbf{w}_x + \mathbf{B}_2(\tilde{\mathbf{v}})\mathbf{w}_y = 0,$$

where

$$\mathbf{B}_1(\tilde{\mathbf{v}}) = \begin{pmatrix} \tilde{u} - \tilde{a} \cos \theta & 0 & -\frac{1}{2}\tilde{a} \sin \theta & 0 \\ 0 & \tilde{u} & 0 & 0 \\ -\tilde{a} \sin \theta & 0 & \tilde{u} & \tilde{a} \sin \theta \\ 0 & 0 & \frac{1}{2}\tilde{a} \sin \theta & \tilde{u} + \tilde{a} \cos \theta \end{pmatrix},$$

$$\mathbf{B}_2(\tilde{\mathbf{v}}) = \begin{pmatrix} \tilde{v} - \tilde{a} \sin \theta & 0 & \frac{1}{2}\tilde{a} \cos \theta & 0 \\ 0 & \tilde{v} & 0 & 0 \\ \tilde{a} \cos \theta & 0 & \tilde{v} & -\tilde{a} \cos \theta \\ 0 & 0 & -\frac{1}{2}\tilde{a} \cos \theta & \tilde{v} + \tilde{a} \sin \theta \end{pmatrix}$$

and the characteristic variables \mathbf{w} are

$$\mathbf{w} = \begin{pmatrix} w_1 \\ w_2 \\ w_3 \\ w_4 \end{pmatrix} = \mathbf{R}^{-1}(\tilde{\mathbf{v}})\mathbf{v} = \begin{pmatrix} \frac{1}{2}\left(-\frac{p}{\tilde{\rho}\tilde{a}} + u \cos \theta + v \sin \theta\right) \\ \rho - \frac{p}{\tilde{a}^2} \\ u \sin \theta - v \cos \theta \\ -\frac{1}{2}\left(\frac{p}{\tilde{\rho}\tilde{a}} + u \cos \theta + v \sin \theta\right) \end{pmatrix}. \quad (2.3)$$

The quasidiagonalized system of the linearized Euler equations has the form

$$\mathbf{w}_t + \begin{pmatrix} \tilde{u} - \tilde{a} \cos \theta & 0 & 0 & 0 \\ 0 & \tilde{u} & 0 & 0 \\ 0 & 0 & \tilde{u} & 0 \\ 0 & 0 & 0 & \tilde{u} + \tilde{a} \cos \theta \end{pmatrix} \mathbf{w}_x + \begin{pmatrix} \tilde{v} - \tilde{a} \sin \theta & 0 & 0 & 0 \\ 0 & \tilde{v} & 0 & 0 \\ 0 & 0 & \tilde{v} & 0 \\ 0 & 0 & 0 & \tilde{v} + \tilde{a} \sin \theta \end{pmatrix} \mathbf{w}_y = \mathbf{S}, \quad (2.4)$$

with

$$\mathbf{S} = \begin{pmatrix} S_1 \\ S_2 \\ S_3 \\ S_4 \end{pmatrix} = \begin{pmatrix} \frac{1}{2}\tilde{a} \left(\sin \theta \frac{\partial w_3}{\partial x} - \cos \theta \frac{\partial w_3}{\partial y} \right) \\ \tilde{a} \sin \theta \left(\frac{\partial w_1}{\partial x} - \frac{\partial w_4}{\partial x} \right) - \tilde{a} \cos \theta \left(\frac{\partial w_1}{\partial y} - \frac{\partial w_4}{\partial y} \right) \\ \frac{1}{2}\tilde{a} \left(-\sin \theta \frac{\partial w_3}{\partial x} + \cos \theta \frac{\partial w_3}{\partial y} \right) \end{pmatrix}.$$

The same procedure had been carried out in [17] for a system form of the wave equation. Actually, we can show that 3×3 system is contained in system (2.2) in the following manner. Set $\tilde{\rho} = 1/\tilde{a}$ and remove the first row corresponding to density, as well as the first column from the Jacobian matrices $\mathbf{A}_1, \mathbf{A}_2$ in (2.2). Then, moving the third equation for pressure into the first row leads to the so-called wave equation system with advection; i.e.,

$$\mathbf{u}_t + \mathbf{A}_1 \mathbf{u}_x + \mathbf{A}_2 \mathbf{u}_y = 0, \quad \mathbf{x} = (x, y)^T \in \mathbb{R}^2, \quad (2.5)$$

where $\mathbf{u} = (p, u, v)^T$ and

$$\mathbf{A}_1 := \begin{pmatrix} \tilde{u} & \tilde{a} & 0 \\ \tilde{a} & \tilde{u} & 0 \\ 0 & 0 & \tilde{u} \end{pmatrix}, \quad \mathbf{A}_2 := \begin{pmatrix} \tilde{v} & 0 & \tilde{a} \\ 0 & \tilde{v} & 0 \\ \tilde{a} & 0 & \tilde{v} \end{pmatrix}.$$

Further, if the advection velocities are $\tilde{u} = \tilde{v} = 0$ and $\tilde{a} = \text{const}$, we get the well-known linear wave equation system, which describes the propagation of acoustic waves. Note that in [17] we did not consider any advection terms. But they are present in the linearized Euler system. These terms lead to more complex configurations that have to be considered in the implementation of our schemes.

The system (2.4) will reduce to a diagonal system, i.e., $S = 0$, only in the special case when the Jacobian matrices $\mathbf{A}_1, \mathbf{A}_2$ commute, which is not the case for the two-dimensional Euler equations.

In what follows we will work with the concept of bicharacteristics. The ℓ th bicharacteristic \mathbf{x}_ℓ corresponding to the ℓ th equation of the system (2.2) is defined by

$$\frac{d\mathbf{x}_\ell}{dt} = \mathbf{b}_{\ell\ell}(\mathbf{n}(\theta)) := (b_{\ell\ell}^1(\mathbf{n}(\theta)), b_{\ell\ell}^2(\mathbf{n}(\theta)))^T, \quad (2.6)$$

with $\mathbf{B}_1 = (b_{jk}^1)_{1 \leq j,k \leq 4}$, $\mathbf{B}_2 = (b_{jk}^2)_{1 \leq j,k \leq 4}$. The set of all bicharacteristics creates the so-called Mach cone (see Fig. 1). We integrate the ℓ th equation of system (2.2) from point $P = (x, y, t + \Delta t)$ down to point $Q_\ell(\theta)$, where the bicharacteristic hits the plane through $P' = (x - \tilde{u}\Delta t, y - \tilde{v}\Delta t, t)$. More precisely, the footpoints of the corresponding bicharacteristics are

$$Q_1(\theta) = (x - (\tilde{u} - \tilde{a} \cos \theta)\Delta t, y - (\tilde{v} - \tilde{a} \sin \theta)\Delta t, t),$$

$$Q_2 = Q_3 = (x - \tilde{u}\Delta t, y - \tilde{v}\Delta t, t),$$

$$Q_4(\theta) = (x - (\tilde{u} + \tilde{a} \cos \theta)\Delta t, y - (\tilde{v} + \tilde{a} \sin \theta)\Delta t, t).$$

Integration of system (2.4) along the bicharacteristics in time gives relations for the characteristic's variables. Now integrating with respect to θ , i.e., over the unit circle, and

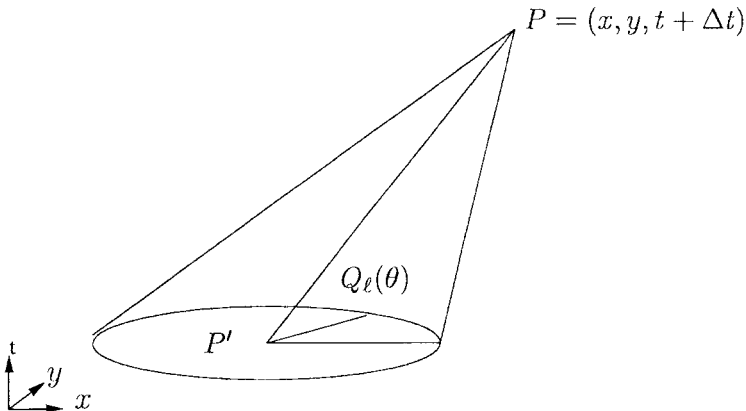


FIG. 1. Bicharacteristics along the Mach cone through P and $Q_\ell(\theta)$.

multiplication from the left by the matrix \mathbf{R} yield the exact integral equation

$$\begin{aligned} \mathbf{v}(P) = & \frac{1}{2\pi} \int_0^{2\pi} \begin{pmatrix} -\frac{\tilde{\rho}}{a} w_1 + w_2 + \frac{\tilde{\rho}}{a} w_4 \\ w_1 \cos \theta + w_3 \sin \theta + w_4 \cos \theta \\ w_1 \sin \theta - w_3 \cos \theta + w_4 \sin \theta \\ -\tilde{\rho} \tilde{a} w_1 + \tilde{\rho} \tilde{a} w_4 \end{pmatrix} d\theta \\ & + \frac{1}{2\pi} \int_0^{2\pi} \begin{pmatrix} -\frac{\tilde{\rho}}{a} S'_1 + \frac{\tilde{\rho}}{a} S'_4 \\ S'_1 \cos \theta + S'_3 \sin \theta + S'_4 \cos \theta \\ S'_1 \sin \theta - S'_3 \cos \theta + S'_4 \sin \theta \\ -\tilde{\rho} \tilde{a} S'_1 + \tilde{\rho} \tilde{a} S'_4 \end{pmatrix} d\theta, \end{aligned} \quad (2.7)$$

where $S'_\ell = \int_t^{t+\Delta t} S_\ell(\mathbf{x}_\ell(\tilde{t}, \theta), \tilde{t}, \theta) d\tilde{t}$ is the time integral along the ℓ th bicharacteristic. In order to avoid a common misconception note that (2.7) is an integral equation for \mathbf{v} and not an integral representation such as the Kirchhoff formula for the wave equation. Note that we must distinguish here between the representation of solution, which is a time explicit formula, and the integral equation for the solution, which is a time implicit formula.

Now we reformulate Eq. (2.7) to enable a numerical implementation. First, note that the relation $Q_1(\theta + \pi) = Q_4(\theta)$ holds. Therefore we have the following symmetries:

$$\begin{aligned} w_1(Q_1(\theta + \pi), \theta + \pi) &= -w_4(Q_4(\theta), \theta), \\ w_1(Q_1(\theta + \pi), \theta + \pi) \cos(\theta + \pi) &= w_4(Q_4(\theta), \theta) \cos(\theta), \\ w_1(Q_1(\theta + \pi), \theta + \pi) \sin(\theta + \pi) &= w_4(Q_4(\theta), \theta) \sin(\theta). \end{aligned}$$

Since all quantities $w_\ell(x, y, t, \theta)$ and $Q_\ell(\theta)$ are 2π -periodic with respect to θ , it follows for the integrals over the basis of the cone (see Fig. 1) that the equations

$$\begin{aligned} - \int_0^{2\pi} w_1(Q_1(\theta), \theta) d\theta &= \int_0^{2\pi} w_4(Q_4(\theta), \theta) d\theta, \\ \int_0^{2\pi} w_1(Q_1(\theta), \theta) \cos(\theta) d\theta &= \int_0^{2\pi} w_4(Q_4(\theta), \theta) \cos(\theta) d\theta, \\ \int_0^{2\pi} w_1(Q_1(\theta), \theta) \sin(\theta) d\theta &= \int_0^{2\pi} w_4(Q_4(\theta), \theta) \sin(\theta) d\theta \end{aligned}$$

hold. Similarly, we have for S'_ℓ the relations

$$\begin{aligned} \int_0^{2\pi} S'_1(\theta) d\theta &= - \int_0^{2\pi} S'_4(\theta) d\theta, \\ \int_0^{2\pi} S'_1(\theta) \cos(\theta) d\theta &= \int_0^{2\pi} S'_4(\theta) \cos(\theta) d\theta, \\ \int_0^{2\pi} S'_1(\theta) \sin(\theta) d\theta &= \int_0^{2\pi} S'_4(\theta) \sin(\theta) d\theta. \end{aligned} \quad (2.8)$$

Because of the θ independence of $Q_2 = Q_3$ the integrals containing $w_2(Q_2(\theta), \theta)$ and

$w_3(Q_3(\theta), \theta)$ can be solved directly. For example, we have the following equalities:

$$\int_0^{2\pi} w_3(Q_3(\theta), \theta) \sin(\theta) d\theta = \pi u(Q_3) \quad \text{and} \quad \int_0^{2\pi} w_3(Q_3(\theta), \theta) \cos(\theta) d\theta = -\pi v(Q_3).$$

Similarly to that in [17, 28] we obtain from (2.7) the following formulae for the exact solution ν of the linearized system at point $P = (\mathbf{x}, t + \Delta t)$. In order to use notation consistent with our previous paper [17] we put $Q := Q_1(\theta)$ and $P' := Q_2$. Then we have

$$\begin{aligned} \rho(\mathbf{x}, t + \Delta t) &= \rho(P') - \frac{p(P')}{\tilde{a}^2} + \frac{1}{2\pi} \int_0^{2\pi} \left[\frac{p(Q)}{\tilde{a}^2} - \frac{\tilde{\rho}}{\tilde{a}} u(Q) \cos \theta - \frac{\tilde{\rho}}{\tilde{a}} v(Q) \sin \theta \right] d\theta \\ &\quad - \frac{\tilde{\rho}}{\tilde{a}} \frac{1}{2\pi} \int_0^{2\pi} \int_t^{t+\Delta t} S(\mathbf{x} - (\tilde{\mathbf{u}} - c\mathbf{n}(\theta))(t + \Delta t - \tilde{t}), \tilde{t}, \theta) d\tilde{t} d\theta, \end{aligned} \quad (2.9)$$

$$\begin{aligned} u(\mathbf{x}, t + \Delta t) &= \frac{1}{2\pi} \int_0^{2\pi} \left[-\frac{p(Q)}{\tilde{\rho}\tilde{a}} \cos \theta + u(Q) \cos^2 \theta + v(Q) \sin \theta \cos \theta \right] d\theta \\ &\quad + \frac{1}{2\pi} \int_0^{2\pi} \int_t^{t+\Delta t} \cos \theta S(\mathbf{x} - (\tilde{\mathbf{u}} - c\mathbf{n}(\theta))(t + \Delta t - \tilde{t}), \tilde{t}, \theta) d\tilde{t} d\theta \\ &\quad + \frac{1}{2} u(P') - \frac{1}{2\tilde{\rho}} \int_t^{t+\Delta t} p_x(P'(\tilde{t})) d\tilde{t}, \end{aligned} \quad (2.10)$$

$$\begin{aligned} v(\mathbf{x}, t + \Delta t) &= \frac{1}{2\pi} \int_0^{2\pi} \left[-\frac{p(Q)}{\tilde{\rho}\tilde{a}} \sin \theta + u(Q) \cos \theta \sin \theta + v(Q) \sin^2 \theta \right] d\theta \\ &\quad + \frac{1}{2\pi} \int_0^{2\pi} \int_t^{t+\Delta t} \sin \theta S(\mathbf{x} - (\tilde{\mathbf{u}} - c\mathbf{n}(\theta))(t + \Delta t - \tilde{t}), \tilde{t}, \theta) d\tilde{t} d\theta \\ &\quad + \frac{1}{2} v(P') - \frac{1}{2\tilde{\rho}} \int_t^{t+\Delta t} p_y(P'(\tilde{t})) d\tilde{t}, \end{aligned} \quad (2.11)$$

$$\begin{aligned} p(\mathbf{x}, t + \Delta t) &= \frac{1}{2\pi} \int_0^{2\pi} [p(Q) - \tilde{\rho}\tilde{a}u(Q) \cos \theta - \tilde{\rho}\tilde{a}v(Q) \sin \theta] d\theta \\ &\quad - \tilde{\rho}\tilde{a} \frac{1}{2\pi} \int_0^{2\pi} \int_t^{t+\Delta t} S(\mathbf{x} - (\tilde{\mathbf{u}} - c\mathbf{n}(\theta))(t + \Delta t - \tilde{t}), \tilde{t}, \theta) d\tilde{t} d\theta, \end{aligned} \quad (2.12)$$

where

$$\begin{aligned} &(\mathbf{x} - (\tilde{\mathbf{u}} - \tilde{a}\mathbf{n}(\theta))(t + \Delta t - \tilde{t})) \\ &= (x - (\tilde{u} - \tilde{a} \cos \theta)(t + \Delta t - \tilde{t}), y - (\tilde{v} - \tilde{a} \sin \theta)(t + \Delta t - \tilde{t})) \end{aligned}$$

and where the so-called source term S is given by

$$\begin{aligned} S(\mathbf{x}, t, \theta) &:= \tilde{a}[u_x(\mathbf{x}, t, \theta) \sin^2 \theta - (u_y(\mathbf{x}, t, \theta) + v_x(\mathbf{x}, t, \theta)) \\ &\quad \times \sin \theta \cos \theta + v_y(\mathbf{x}, t, \theta) \cos^2 \theta]. \end{aligned} \quad (2.13)$$

Note that we have derived an exact integral equation for the solution to the linearized Euler equations (2.2). This will be a basis for our further numerical approximations. The time integrals of S are the terms needing most attention. In the next section we shall use quadratures in time to construct approximate evolution operators.

2.2. Approximate Evolution Operators

As in [17] the integrals of the source term with respect to time will be approximated by the rectangle rule or by the trapezoidal rule. They lead to an $O(\Delta t)$ or $O(\Delta t^2)$ approximation, respectively. In both cases we would need to evaluate derivatives of the velocity components at time t . However, in [17, Lemma 2.1] we found that the integrals of the source S can be simplified through integration by parts, which yields

$$\Delta t \int_0^{2\pi} S(t, \theta) d\theta = \int_0^{2\pi} [u_Q \cos \theta + v_Q \sin \theta] d\theta. \quad (2.14)$$

Analogously, we can derive the formulae

$$\Delta t \int_0^{2\pi} S(t, \theta) \sin \theta d\theta = \int_0^{2\pi} [2u_Q \sin \theta \cos \theta + v_Q(2 \sin^2 \theta - 1)] d\theta \quad (2.15)$$

and

$$\Delta t \int_0^{2\pi} S(t, \theta) \cos \theta d\theta = \int_0^{2\pi} [u_Q(2 \cos^2 \theta - 1) + 2v_Q \sin \theta \cos \theta] d\theta. \quad (2.16)$$

Let us first apply the rectangle rule to the exact integral representation (2.9)–(2.12). As in [17] the integrals in (2.10) and (2.11) involving p_x and p_y need to be replaced by integrals over the cone mantle. This is done by using the Gauss theorem (see [17]). In this way we have generated the approximate evolution operator, which we, analogously to that in [17], call the EG3 operator.

Approximate evolution operator EG3.

$$\begin{aligned} \rho(P) &= \rho(P') - \frac{p(P')}{\tilde{a}^2} + \frac{1}{2\pi} \int_0^{2\pi} \left[\frac{p(Q)}{\tilde{a}^2} - 2\frac{\tilde{\rho}}{\tilde{a}} u(Q) \cos \theta - 2\frac{\tilde{\rho}}{\tilde{a}} v(Q) \sin \theta \right] d\theta \\ &\quad + O(\Delta t^2), \end{aligned} \quad (2.17)$$

$$\begin{aligned} u(P) &= \frac{1}{2} u(P') + \frac{1}{2\pi} \int_0^{2\pi} \left[-\frac{2}{\tilde{\rho}\tilde{a}} p(Q) \cos \theta + u(Q)(3 \cos^2 \theta - 1) + 3v(Q) \sin \theta \cos \theta \right] d\theta \\ &\quad + O(\Delta t^2), \end{aligned} \quad (2.18)$$

$$\begin{aligned} v(P) &= \frac{1}{2} v(P') + \frac{1}{2\pi} \int_0^{2\pi} \left[-\frac{2}{\tilde{\rho}\tilde{a}} p(Q) \sin \theta + 3u(Q) \sin \theta \cos \theta + v(Q)(3 \sin^2 \theta - 1) \right] d\theta \\ &\quad + O(\Delta t^2), \end{aligned} \quad (2.19)$$

$$p(P) = \frac{1}{2\pi} \int_0^{2\pi} [p(Q) - 2\tilde{\rho}\tilde{a}u(Q) \cos \theta - 2\tilde{\rho}\tilde{a}v(Q) \sin \theta] d\theta + O(\Delta t^2), \quad (2.20)$$

where $Q = (x - \Delta t(\tilde{u} - \tilde{a} \cos \theta), y - \Delta t(\tilde{v} - \tilde{a} \sin \theta), t)$, $P' = (x - \Delta t\tilde{u}, y - \Delta t\tilde{v}, t)$, and $P = (x, y, t + \Delta t)$. This is the approximate evolution operator that gave us, for the wave equation system, the best results in general. In [17] also the EG1 and the EG2 approximate evolution operators were studied. For the sake of completeness we derive here the other two approximate evolution operators for the Euler equations. Our numerical experiments for the linear wave equation system [18] as well as for the nonlinear Euler equations show that the second-order FVEG1 and FVEG3 schemes lead to comparable results, whereas the FVEG2 scheme gives larger errors.

Now we reformulate the integral equations (2.10), (2.11) for u and v , respectively. Using the second and third equation of the linearized system (2.2) we can replace terms involving

integrals of p_x or p_y and $u(P')$ or $v(P')$ by means of $u(P)$ or $v(P)$, respectively. Thus we have the following equivalent exact integral equations for $u(P)$ and $v(P)$, respectively:

$$\begin{aligned} u(\mathbf{x}, t + \Delta t) &= \frac{1}{\pi} \int_0^{2\pi} \left[-\frac{p(Q)}{\tilde{\rho}\tilde{a}} \cos \theta + u(Q) \cos^2 \theta + v(Q) \sin \theta \cos \theta \right] d\theta \\ &\quad + \frac{1}{\pi} \int_0^{2\pi} \int_t^{t+\Delta t} \cos \theta S(\mathbf{x} - (\tilde{\mathbf{u}} - c\mathbf{n}(\theta))(t + \Delta t - \tilde{t}), \tilde{t}, \theta) d\tilde{t} d\theta, \\ v(\mathbf{x}, t + \Delta t) &= \frac{1}{\pi} \int_0^{2\pi} \left[-\frac{p(Q)}{\tilde{\rho}\tilde{a}} \sin \theta + u(Q) \cos \theta \sin \theta + v(Q) \sin^2 \theta \right] d\theta \\ &\quad + \frac{1}{\pi} \int_0^{2\pi} \int_t^{t+\Delta t} \sin \theta S(\mathbf{x} - (\tilde{\mathbf{u}} - c\mathbf{n}(\theta))(t + \Delta t - \tilde{t}), \tilde{t}, \theta) d\tilde{t} d\theta. \end{aligned} \quad (2.21)$$

Now, applying the rectangle rule in order to approximate the source terms in (2.21) and applying (2.15), (2.16) leads to the following approximate evolution formulae for the velocity components. These are a part of the approximate evolution operator which we refer to as the EG1. The approximate evolution formulae for ρ and p are the same as for the EG3 operator, i.e., (2.17), (2.20).

Approximate evolution operator EG1.

$$u(P) = \frac{1}{\pi} \int_0^{2\pi} -\frac{p(Q)}{\tilde{\rho}\tilde{a}} \cos \theta + u(Q)(3 \cos^2 \theta - 1) + 3v(Q) \sin \theta \cos \theta d\theta + O(\Delta t^2), \quad (2.22)$$

$$v(P) = \frac{1}{\pi} \int_0^{2\pi} -\frac{p(Q)}{\tilde{\rho}\tilde{a}} \sin \theta + 3u(Q) \sin \theta \cos \theta + v(Q)(3 \sin^2 \theta - 1) d\theta + O(\Delta t^2). \quad (2.23)$$

Finally, we apply the trapezoidal rule to approximate integrals of the source terms with respect to time in the integral equations (2.9), (2.21), and (2.12). This leads to the following approximations:

$$\begin{aligned} \frac{1}{2\pi} \int_t^{t+\Delta t} \int_0^{2\pi} S(\tilde{t}, \theta) d\theta d\tilde{t} &= \frac{1}{2} \Delta t \left[\frac{1}{2\pi} \int_0^{2\pi} S(t + \Delta t, \theta) d\theta + \frac{1}{2\pi} \int_0^{2\pi} S(t, \theta) d\theta \right] \\ &\quad + O(\Delta t^3) \\ &= \frac{1}{2} \Delta t \left[\frac{1}{2} \tilde{a}(u_x + v_y)_P + \frac{1}{2\pi} \int_0^{2\pi} S(t, \theta) d\theta \right] + O(\Delta t^3), \end{aligned} \quad (2.24)$$

$$\begin{aligned} \frac{1}{\pi} \int_t^{t+\Delta t} \int_0^{2\pi} S(\tilde{t}, \theta) \cos(\theta) d\theta d\tilde{t} &= \frac{1}{2} \Delta t \left[\frac{1}{\pi} \int_0^{2\pi} S(t + \Delta t, \theta) \cos(\theta) d\theta \right. \\ &\quad \left. + \frac{1}{\pi} \int_0^{2\pi} S(t, \theta) \cos(\theta) d\theta \right] + O(\Delta t^3) \\ &= \Delta t \frac{1}{2\pi} \int_0^\pi S(t, \theta) \cos(\theta) d\theta + O(\Delta t^3). \end{aligned} \quad (2.25)$$

Note that for the $S \cos \theta$ term the integral at the apex P of the Mach cone vanishes. An analogous formula to (2.25) holds for $S \sin \theta$.

However, now we have introduced in (2.24) the unknown derivatives u_x and v_y at the apex P for which we want to solve. Following Butler's ideas [4] we solved this problem for the wave equation system in [17] and derived the so-called EG2 approximate evolution operator. Here, we will analogously eliminate these derivatives via integration of the equations for ρ and p along a bicharacteristic curve $P'P$. Thus, using the same trapezoidal rule to integrate the first and the last equation of (2.2) from P' to P gives

$$\rho_P - \rho_{P'} + \frac{1}{2} \Delta t \tilde{\rho} [(u_x + v_y)_P + (u_x + v_y)_{P'}] = O(\Delta t^3), \quad (2.26)$$

$$p_P - p_{P'} + \frac{1}{2} \Delta t \tilde{\rho} \tilde{a}^2 [(u_x + v_y)_P + (u_x + v_y)_{P'}] = O(\Delta t^3), \quad (2.27)$$

respectively. Using (2.26) or (2.27) we eliminate the derivatives at the apex P of the Mach cone but still introduce the derivatives at point P' . Now, similarly to that for the integrals of p_x, p_y in the derivation of the EG3 operator, we apply the Gauss theorem to replace u_x and v_y at point P' by terms over the cone mantle. More precisely, we obtain

$$\begin{aligned} \pi(c\Delta t)^2(u_x + v_y)_{P'} &= \int_O (u_x + v_y) dx dy + O(\Delta t^4) = \oint [u dy - v dx] + O(\Delta t^4) \\ &= c\Delta t \int_0^{2\pi} [u_Q \cos \theta + v_Q \sin \theta] d\theta + O(\Delta t^4). \end{aligned} \quad (2.28)$$

Combining the exact formulae (2.9), (2.21), (2.12) with the approximations (2.24), (2.25), (2.26), (2.27), (2.28), as well as with (2.14), (2.15), (2.16), yields the approximate evolution operator, which we, analogously to that in [17], call the EG2.

Approximate evolution operator EG2.

$$\rho(P) = \rho(P') - 2 \frac{p(P')}{\tilde{a}^2} + \frac{1}{\pi} \int_0^{2\pi} \left[\frac{p(Q)}{\tilde{a}^2} - \frac{\tilde{\rho}}{\tilde{a}} u(Q) \cos \theta - \frac{\tilde{\rho}}{\tilde{a}} v(Q) \sin \theta \right] d\theta, \quad (2.29)$$

$$u(P) = \frac{1}{\pi} \int_0^\pi \left[-\frac{p(Q)}{\tilde{\rho} \tilde{a}} \cos \theta + u(Q)(2 \cos^2 \theta - 1/2) + 2v(Q) \sin \theta \cos \theta \right] d\theta, \quad (2.30)$$

$$v(P) = \frac{1}{\pi} \int_0^{2\pi} \left[-\frac{p(Q)}{\tilde{\rho} \tilde{a}} \sin \theta + 2u(Q) \cos \theta \sin \theta + v(Q)(2 \sin^2 \theta - 1/2) \right] d\theta, \quad (2.31)$$

$$p(P) = -p(P') + \frac{1}{\pi} \int_0^{2\pi} [p(Q) - \tilde{\rho} \tilde{a} u(Q) \cos \theta - \tilde{\rho} \tilde{a} v(Q) \sin \theta] d\theta. \quad (2.32)$$

3. FINITE VOLUME EVOLUTION GALERKIN SCHEMES

Our first attempt to use the multidimensional approximate evolution operators in numerical schemes led us to try the evolution Galerkin approach. There piecewise polynomial data are evolved using approximate evolution operators of the kind derived in the previous section. After each time step the solution is projected back onto the piecewise polynomials with respect to the mesh. For piecewise constant functions, this had already turned out to involve quite tedious calculations. It was barely feasible for practical applications. Even after some

simplifications concerning the evaluation of the multiple integrals that appeared, we came to the conclusion that in order to go to higher order, a different approach was to be taken. The approximate evolution of nonconstant data is just too complicated. The decisive step that we took was to go to the finite volume framework. We believe that the finite volume approach is highly advantageous in practical applications because conservativity is automatically guaranteed and it is relatively easy to go to higher order via standard recovery procedures. In finite volume methods the approximate evolutions are used to evaluate the numerical fluxes. We give a short outline of the finite volume approach to fix notations and then introduce the recovery procedures that we have considered for our schemes. Finally, we show how to proceed for nonlinear systems by considering the Euler equations of gas dynamics.

Now we will describe finite volume evolution Galerkin (FVEG) schemes for a general hyperbolic system in d space dimensions; i.e.,

$$\mathbf{u}_t + \sum_{k=1}^d (\mathbf{f}_k(\mathbf{u}))_{x_k} = 0, \quad \mathbf{x} = (x_1, \dots, x_d)^T \in \mathbb{R}^d, \quad (3.1)$$

where $\mathbf{f}_k = \mathbf{f}_k(\mathbf{u})$, $k = 1, \dots, d$ represent given physical flux functions and the conservative variables are $\mathbf{u} = (u_1, \dots, u_m)^T \in \mathbb{R}^m$. Denote by $E(s) : X \rightarrow X$ the exact evolution operator associated with a time step s acting on some suitable function space X for system (3.1); i.e.,

$$\mathbf{u}(\cdot, t + s) = E(s)\mathbf{u}(\cdot, t). \quad (3.2)$$

Let Ω be our two-dimensional computational domain. We construct a mesh for Ω , which consists of the square mesh cells

$$\begin{aligned} \Omega_{ij} &\equiv \left[\left(i - \frac{1}{2} \right) h, \left(i + \frac{1}{2} \right) h \right] \times \left[\left(j - \frac{1}{2} \right) h, \left(j + \frac{1}{2} \right) h \right] \\ &= [x_{i-1/2}, x_{i+1/2}] \times [y_{j-1/2}, y_{j+1/2}], \end{aligned}$$

where $i, j \in \mathbb{Z}$ and $h > 0$ is the mesh size parameter.

We suppose that S_h^p is a finite element space consisting of piecewise polynomials of degree $p \geq 0$. Let \mathbf{U}^n be an approximation in the space S_h^p to the exact solution $\mathbf{u}(\cdot, t_n)$ at a time $t_n > 0$ and take $E_\tau : S_h^p \rightarrow X$ to be a suitable approximation to the exact evolution operator $E(\tau)$, $r > 0$. We denote by $R_h : S_h^p \rightarrow S_h^r$ a recovery operator, $r > p \geq 0$. For simplicity we shall limit our considerations to cases of constant time step Δt , i.e., $t_n = n\Delta t$, and of a uniform mesh consisting of d -dimensional cubes with a uniform mesh size h . However, generalization to nonuniform meshes can be made and it is only a question of implementation. Morton [25] gave an error analysis of the finite volume evolution Galerkin schemes for scalar conservation laws for arbitrary meshes.

DEFINITION 3.1. Starting from some initial value \mathbf{U}^0 at time $t = 0$, the finite volume evolution Galerkin method (FVEG) is recursively defined by means of

$$\mathbf{U}^{n+1} = \mathbf{U}^n - \frac{1}{h} \int_0^{\Delta t} \sum_{k=1}^d \delta_{x_k} \mathbf{f}_k(\mathbf{U}^{n+\tau/\Delta t}) d\tau, \quad (3.3)$$

where the central difference $v(x + h/2) - v(x - h/2)$ is denoted by $\delta_x v(x)$ and

$\delta_{x_k} f_k(\mathbf{U}^{n+\tau/\Delta t})$ represents an approximation to the edge flux difference at intermediate time levels $t_n + \tau$, $\tau \in]0, \Delta t[$. The cell boundary flux $f_k(\mathbf{U}^{n+\tau/\Delta t})$ is evolved using the approximate evolution operator E_τ to $t_n + \tau$ and averaged along the cell boundary; for example, on the right-hand vertical edge $\mathcal{E}_{i+1/2} := \{[x_{i+1/2}, y], y \in [(j-1/2)h, (j+1/2)h]\}$ we have

$$f_k(\mathbf{U}^{n+\tau/\Delta t}) = \frac{1}{h} \int_{\mathcal{E}_{i+1/2}} f_k(E_\tau R_h \mathbf{U}^n) dS_y. \quad (3.4)$$

This is the new key step in our FVEG method. An analogous formula holds for the left-hand side edge $\mathcal{E}_{i-1/2,j}$ as well as for horizontal edges $\mathcal{E}_{i,j\pm 1/2}$.

For the computation of fluxes on cell interfaces the value of \mathbf{U} has to be determined by means of an approximate evolution operator. We approximate the time integral in (3.3) by the midpoint rule.

If no recovery is used the whole method is of first order. In this case the finite volume evolution Galerkin scheme (3.3), (3.4) reads

$$\mathbf{U}^{n+1} = \mathbf{U}^n - \frac{\Delta t}{h} \sum_{k=1}^d \delta_{x_k} f_k(\mathbf{U}^*), \quad (3.5)$$

$$f_k(\mathbf{U}^*) = \frac{1}{h} \int_{\mathcal{E}} f_k(E_{\Delta t/2} \mathbf{U}^n) dS, \quad (3.6)$$

where the integration in (3.6) is done for every edge \mathcal{E} of the corresponding control volume. However, the most important advantage of the above finite volume formulation (3.3), (3.4) is that even a first-order-accurate approximation E_τ to the evolution operator $E(\tau)$ yields an overall second-order update from \mathbf{U}^n to \mathbf{U}^{n+1} if the recovery operator is applied. The second-order scheme is obtained by a conservative discontinuous bilinear recovery using the vertex values. Thus the fluxes are computed using the intermediate solution on cell interface:

$$f_k(\mathbf{U}^*) = \frac{1}{h} \int_{\mathcal{E}} f_k(E_{\Delta t/2} R_h \mathbf{U}^n) dS. \quad (3.7)$$

3.1. Bilinear Recovery and Limiters

There are many possible recovery schemes on piecewise constant data, with respect to the mesh, which could be used. One possibility, which we chose for our numerical computations, is discontinuous bilinear recovery using finite difference approximation of derivatives. It is taken to be conservative and given as

$$R_h \mathbf{U}|_{\Omega_{ij}} = \left(1 + \frac{(x-x_i)}{h} \mu_x \mu_y^2 \delta_x + \frac{(y-y_j)}{h} \mu_x^2 \mu_y \delta_y + \frac{(x-x_i)(y-y_j)}{h^2} \mu_x \mu_y \delta_x \delta_y \right) \mathbf{U}_{ij}, \quad (3.8)$$

where $\mu_x v(x) = \frac{1}{2}(v(x+h) + v(x-h))$ and where an analogous notation is used for y -direction. In order to avoid developing oscillations in the solution the gradients of this bilinear recovery are multiplied by limiters. We have tested a minmod-type limiter (see Barth and Jespersen [1]). Let U^ℓ , with $\ell = 1, 2, \dots, m$, denote any component of the

vector \mathbf{U} . For example, the limiter at an upper right vertex $(i + 1/2, j + 1/2)$ is computed for each component by

$$\Phi_\ell = \begin{cases} 1, & \text{if } \tilde{U}^\ell = U_{ij}^\ell, \\ \min(1, (U^{\ell_{max}} - U_{ij}^\ell)/(\tilde{U}^\ell - U_{ij}^\ell)), & \text{if } \tilde{U}^\ell > U_{ij}^\ell, \\ \min(1, (U^{\ell_{min}} - U_{ij}^\ell)/(\tilde{U}^\ell - U_{ij}^\ell)), & \text{if } \tilde{U}^\ell < U_{ij}^\ell, \end{cases} \quad (3.9)$$

where $\tilde{U}^\ell = (R_h U^\ell)_{i+1/2, j+1/2}$ and $U^{\ell_{min}}, U^{\ell_{max}}$ are local extrema at the vertex $(i + 1/2, j + 1/2)$ computed from $U_{i+1, j+1}^\ell, U_{i+1, j}^\ell, U_{i, j+1}^\ell, U_{ij}^\ell$. The limiting is done for each component of the vector \mathbf{U} separately. In the case of the Euler equations we work here with the primitive variables vector; i.e., $\mathbf{U} = (\rho, u, v, p)^\top$. As a result, a new limited form of the piecewise bilinear recovery (3.8) is given, for example at the vertex $(x_{i+1/2}, y_{j+1/2})$, as follows:

$$(R_h \mathbf{U})_{i+1/2, j+1/2}^L = \mathbf{U}_{ij} + \Phi \left[\left(\frac{1}{2} \mu_x \mu_y^2 \delta_x + \frac{1}{2} \mu_x^2 \mu_y \delta_y + \frac{1}{4} \mu_x \mu_y \delta_x \delta_y \right) \mathbf{U}_{ij} \right]. \quad (3.10)$$

Another possibility, which we also tested experimentally, is to approximate the x -, y -, and xy - slopes by means of recovery with the classical minmod slope limiter or the WENO recovery. For example, the x - slope U_x of $R_h \mathbf{U}$ at the mesh cell Ω_{ij} is given as

$$U_x := \frac{1}{h} \Psi(\mathbf{U}_{i+1, j} - \mathbf{U}_{ij}, \mathbf{U}_{ij} - \mathbf{U}_{i-1, j}). \quad (3.11)$$

For the classical minmod recovery it holds that

$$\Psi_\ell(a, b) = \text{minmod}(a, b) \equiv 1/2(\text{sgn}(a) + \text{sgn}(b))\min(|a|, |b|), \quad a, b \in \mathbb{R}, \quad (3.12)$$

for each component $\ell = 1, 2, \dots, m$ of the operator Ψ . For the WENO recovery,

$$\Psi_\ell(a, b) = \text{WENO}(a, b) \equiv (\omega_1 a + \omega_2 b)/(\omega_1 + \omega_2), \quad (3.13)$$

with $\omega_1 = (\mathcal{E} + a^2)^{-2}$, $\omega_2 = (\mathcal{E} + b^2)^{-2}$. As in [12] \mathcal{E} is taken to be 10^{-6} .

In our calculations in Section 5 we have used (3.12), but our numerical comparisons with the other limiting techniques, (3.9) and (3.13), show only marginal differences.

3.2. Euler Equations

We have applied the above general definition very successfully to linear problems, e.g., the wave equation system. The applications to the linear Maxwell equations were recently explored (see [24, 32]). In [18–20] we presented several results of numerical experiments and showed that the above approach led to very accurate schemes under the comparable computational cost of other commonly used schemes. For example, in comparison with the Lax–Wendroff scheme (rotated-Richtmyer version), the second-order FVEG1 method is seven times more accurate (see [19]). For linear problems the EG methods capture multidimensional effects such as rotational symmetry, circular shocks, and preservation of vorticity very well (see [17–19]). The aim of this paper is to apply finite volume evolution Galerkin methods to nonlinear problems, particularly to the Euler equation systems.

The finite volume formulation, which automatically implies the conservativity property, works with the conservation form of the Euler equations; i.e.,

$$\mathbf{u}_t + \mathbf{f}_1(\mathbf{u})_x + \mathbf{f}_2(\mathbf{u})_y = 0, \quad (3.14)$$

where the vector of conservative variables and the fluxes are

$$\mathbf{u} := \begin{pmatrix} \rho \\ \rho u \\ \rho v \\ e \end{pmatrix}, \quad \mathbf{f}_1(\mathbf{u}) := \begin{pmatrix} \rho u \\ \rho u^2 + p \\ \rho uv \\ (e + p)u \end{pmatrix}, \quad \mathbf{f}_2(\mathbf{u}) := \begin{pmatrix} \rho v \\ \rho uv \\ \rho v^2 + p \\ (e + p)v \end{pmatrix}.$$

Here, e stands for the total energy; i.e., $e = p/(\gamma - 1) + \rho(u^2 + v^2)/2$. However, in Section 2.1, in order to consider bicharacteristics and to derive approximate evolution operators, it was easier to work equivalently with the system in primitive variables $\mathbf{v} = (\rho, u, v, p)$. Thus, for the Euler equations we will work in (3.7) with the vector of primitive variables \mathbf{v} instead of the vector of conservative variables \mathbf{u} . This latter is only used in the finite volume form (3.5) to maintain conservativity at discontinuities. Note also that the limiting procedures, which are described in the previous subsection, are applied to a vector in primitive variables.

In order to compute fluxes on cell interfaces by means of the approximate evolution operator, we need to evaluate integrals along the cell interface and around the Mach cone (cf. (3.6), (3.7)). There are generally two ways to do this: integrals can be evaluated either exactly or by means of a suitable numerical quadrature. We have tested each possibility with respect to stability and accuracy from an experimental as well as theoretical point of view.

Let us discuss the implementation aspect. In the case of the first- and second-order scheme for the wave equation system without advection, as well as in the case of the first-order scheme for the Euler equations, we have evaluated and implemented both integrals around the Mach cone and along the cell interface exactly as well as numerically. However, for configurations with slanted Mach cones, e.g., the Euler equations, exact evaluation of both integrals leads to very lengthy and tedious computations, especially when higher order polynomial approximations are used. In order to simplify the derivation and implementation of the second-order scheme for the Euler equations, we approximated cell interface integrals using the Simpson rule and evaluated fluxes at vertices and midpoints. For our forthcoming paper [22] we are studying several possible numerical quadratures for discontinuous functions. It is proved in [22] that the Simpson rule leads to a scheme which is monotonic under some conditions. Moreover, it takes multidimensional effects from the corners into account. On the other hand, the trapezoidal rule leads to nonmonotonic schemes and oscillations in solutions. We will demonstrate this fact in our numerical experiments in Section 5. Let us consider a natural CFL number, $\nu = \max(|u| + c, |v| + c)\Delta t/h \leq 1$. Then the midpoint rule approximation of cell interface integrals naturally does not take into account corner effects, since the fluxes are evaluated at $t_n + \Delta t/2$. Therefore this quadrature rule is inappropriate for a multidimensional scheme.

For the Mach cone integral both evaluations, i.e., the trapezoidal rule approximation as well as the exact computation, have been implemented. For a numerical integration we take a trapezoidal rule, since it has constant weights, which is very suitable for the periodic

functions appearing in the approximate evolution operators (see also [11] for more details on numerical integration).

In order to construct local Mach cones we need to define the local velocities of the flow (\tilde{u}, \tilde{v}) as well as the local speed of sound \tilde{a} . Note that for linear problems these functions are given. This local flow information can be computed, for example, by an averaging process. If the cell interface integral is computed exactly, the averaging is done over six cells adjacent to the edge considered. Otherwise, if the Simpson rule is used, we average over four cells adjacent to the vertex or over two cells adjacent to the midpoint, respectively.

In this case the linearization is done at time $\tilde{t} = t_n$. However, in order to construct higher order schemes, we will show in Lemma 4.1 that the Jacobian matrices have to be frozen at the half time $\tilde{t} = t_n + \Delta t/2$. For example, if the exact evaluation is used we have to predict, for example for the right-hand edge $\mathcal{E}_{i+1/2} := \{[x_{i+1/2}, y], y \in [(j-1/2)h, (j+1/2)h]\}$, the values

$$\begin{aligned}\tilde{u} &:= \tilde{u}\left(x_{i+1/2}, y_j, t_n + \frac{1}{2}\Delta t\right), \\ \tilde{v} &:= \tilde{v}\left(x_{i+1/2}, y_j, t_n + \frac{1}{2}\Delta t\right), \\ \tilde{a} &:= \tilde{a}\left(x_{i+1/2}, y_j, t_n + \frac{1}{2}\Delta t\right)\end{aligned}\tag{3.15}$$

Now, being at time t_n we have no information about the solution there. Therefore, a predictor step is needed to compute the solution at $t_n + \Delta t/2$. In our computations we have used the Lax–Friedrichs method to compute this auxiliary information. This gives us the desired local flow velocities, which are computed either at the midpoints of cell interfaces or at the vertices, depending on the integral evaluation. We have also experimented with taking the simple averages of adjacent states at time t_n as predicted values in conjunction with quadrature rules. This is less expensive and works as well. According to Corollary 4.2 we can also compute local velocities $\tilde{u}, \tilde{v}, \tilde{a}$ in the predictor step for the time $\tilde{t} = t_n + \Delta t$, which gives only a first-order linearization error in time.

4. ERROR ANALYSIS OF THE FVEG SCHEMES

The aim of this section is to analyze error estimates for the FVEG schemes. We will be particularly interested to show error estimates for the second-order version of the FVEG schemes (3.5), (3.7), but we also make remarks about the first-order error of the FVEG method (3.5), (3.6). First, we consider the linearization error in time, which is made if a fully nonlinear hyperbolic system is approximated by a linear variable coefficient system by freezing the time variable in the coefficient matrices. In Section 4.2 we study the global error in space and time. We show how, for a general nonlinear hyperbolic system, it depends on the stability of the scheme as well as on the truncation error. In Section 4.3 we study the truncation error. We restrict our analysis to the case of linear constant coefficient hyperbolic systems. Note that we do not discuss here effects of the linearization in space. Our analysis is presented under the assumption that the linearization is chosen in such a way that the resulting numerical scheme is strongly stable (cf. (4.16)). The error analysis for fully nonlinear hyperbolic systems remains an open problem. One additional difficulty will be the occurrence of sonic points and consistency with the entropy inequality.

4.1. The Linearization Error in Time

In this section our aim is to analyze the linearization error, which we make if we replace nonlinear system (2.1) with the linearized system (2.2). Here, we will consider only the error in time. The whole error of the numerical scheme, i.e., error in space and time, will be discussed in Section 4.2.

Our next lemma shows that by freezing the Jacobian matrices at the half time step $\tilde{t} = t_n + \Delta t/2$, we obtain a second-order-accurate linearization. For simplicity in notation we denote the solution of the linearized system by \mathbf{w} .

LEMMA 4.1. *Let \mathbf{w} be a solution to the linearized system*

$$\begin{aligned}\mathbf{w}_t + \tilde{\mathbf{A}}_1 \mathbf{w}_x + \tilde{\mathbf{A}}_2 \mathbf{w}_y &= 0, \\ \mathbf{w}(t_n) &= \mathbf{v}(t_n),\end{aligned}\tag{4.1}$$

where

$$\tilde{\mathbf{A}}_k(\mathbf{x}) = \tilde{\mathbf{A}}_k(\mathbf{x}, t_n + \Delta t/2), \quad k = 1, 2.\tag{4.2}$$

Then the error of linearization is of second order; i.e.,

$$\mathbf{v}(t_n + \Delta t) - \mathbf{w}(t_n + \Delta t) = \mathcal{O}(\Delta t^3).\tag{4.3}$$

Proof. We expand the solutions \mathbf{v} and \mathbf{w} into Taylor series and compute their time derivatives at $t = t_n$:

$$\begin{aligned}\mathbf{v}_t &= -\mathbf{A}_1(\mathbf{v})\mathbf{v}_x - \mathbf{A}_2(\mathbf{v})\mathbf{v}_y, \\ \mathbf{v}_{tt} &= -\partial_t(\mathbf{A}_1(\mathbf{v}))\mathbf{v}_x - \mathbf{A}_1(\mathbf{v})\mathbf{v}_{xt} - \partial_t(\mathbf{A}_2(\mathbf{v}))\mathbf{v}_y - \mathbf{A}_2(\mathbf{v})\mathbf{v}_{yt}, \\ \mathbf{w}_t &= -\tilde{\mathbf{A}}_1 \mathbf{w}_x - \tilde{\mathbf{A}}_2 \mathbf{w}_y = -\tilde{\mathbf{A}}_1 \mathbf{v}_x - \tilde{\mathbf{A}}_2 \mathbf{v}_y, \\ \mathbf{w}_{tt} &= -\tilde{\mathbf{A}}_1 \mathbf{w}_{xt} - \tilde{\mathbf{A}}_2 \mathbf{w}_{yt} \\ &= -\mathbf{A}_1(\mathbf{v})\mathbf{w}_{xt} - \mathbf{A}_2(\mathbf{v})\mathbf{w}_{yt} + \mathcal{O}(\Delta t).\end{aligned}\tag{4.4}$$

Subtracting the derivatives of \mathbf{v} and \mathbf{w} we have the relations

$$\begin{aligned}\mathbf{v}_t - \mathbf{w}_t &= (\tilde{\mathbf{A}}_1 - \mathbf{A}_1(\mathbf{v}))\mathbf{v}_x + (\tilde{\mathbf{A}}_2 - \mathbf{A}_2(\mathbf{v}))\mathbf{v}_y \\ &= \Delta t/2[\partial_t(\mathbf{A}_1(\mathbf{v}))\mathbf{v}_x + \partial_t(\mathbf{A}_2(\mathbf{v}))\mathbf{v}_y] + \mathcal{O}(\Delta t^2)\end{aligned}\tag{4.5}$$

and

$$\begin{aligned}\mathbf{v}_{tt} - \mathbf{w}_{tt} &= -\mathbf{A}_1(\mathbf{v})\partial_x(\mathbf{v}_t - \mathbf{w}_t) - \mathbf{A}_2(\mathbf{v})\partial_y(\mathbf{v}_t - \mathbf{w}_t) - \partial_t \mathbf{A}_1(\mathbf{v})\mathbf{v}_x - \partial_t \mathbf{A}_2(\mathbf{v})\mathbf{v}_y + \mathcal{O}(\Delta t) \\ &= -\partial_t(\mathbf{A}_1(\mathbf{v}))\mathbf{v}_x - \partial_t(\mathbf{A}_2(\mathbf{v}))\mathbf{v}_y + \mathcal{O}(\Delta t).\end{aligned}\tag{4.6}$$

Plugging (4.5) and (4.6) into the Taylor expansion for $\mathbf{v}(t_n + \Delta t) - \mathbf{w}(t_n + \Delta t)$ yields

$$\begin{aligned}\mathbf{v}(t_n + \Delta t) - \mathbf{w}(t_n + \Delta t) &= \Delta t(\mathbf{v}_t - \mathbf{w}_t) + \Delta t^2/2(\mathbf{v}_{tt} - \mathbf{w}_{tt}) + \mathcal{O}(\Delta t^3) \\ &= \Delta t^2/2(\partial_t \mathbf{A}_1(\mathbf{v})\mathbf{v}_x + \partial_t \mathbf{A}_2(\mathbf{v})\mathbf{v}_y) \\ &\quad - \Delta t^2/2(\partial_t \mathbf{A}_1(\mathbf{v})\mathbf{v}_x + \partial_t \mathbf{A}_2(\mathbf{v})\mathbf{v}_y) + \mathcal{O}(\Delta t^3) \\ &= \mathcal{O}(\Delta t^3).\end{aligned}$$

It is easy to see from the proof above that the following corollary holds.

COROLLARY 4.2. *Let \mathbf{w} be a solution to the linearized system (4.1), where the Jacobian matrices are frozen either at time t_n ,*

$$\tilde{\mathbf{A}}_k(\mathbf{x}) = \tilde{\mathbf{A}}_k(\mathbf{x}, t_n), \quad k = 1, 2, \quad (4.7)$$

or at time $t_n + \Delta t$,

$$\tilde{\mathbf{A}}_k(\mathbf{x}) = \tilde{\mathbf{A}}_k(\mathbf{x}, t_n + \Delta t), \quad k = 1, 2. \quad (4.8)$$

Then the linearization error is of first order in time; i.e.,

$$\mathbf{v}(t_n + \Delta t) - \mathbf{w}(t_n + \Delta t) = \mathcal{O}(\Delta t^2). \quad (4.9)$$

Let us note that our Jacobian matrices now depend only on the space variables \mathbf{x} . In practice, similarly to that in the MOT-ICE scheme of Noelle [27], they are evaluated by a predictor step at time $t_n + \Delta t/2$ for the second-order scheme. For the first-order scheme we have two possibilities for freezing time in order to linearize Jacobian matrices, which can be chosen freely, depending only on what problem we solve.

4.2. The Global Error

We rewrite our FVEG method (3.5), (3.7) in more-compact form as

$$\mathbf{U}^{n+1} = \mathcal{N}_h R_h \mathbf{U}^n, \quad (4.10)$$

where \mathcal{N}_h denotes the FVEG update. Suppose \mathbf{U} is some smooth function that is approximated by a piecewise constant step function with respect to the mesh, e.g., obtained by projection or taking cell midpoint values. A conservative piecewise bilinear recovery R_h of \mathbf{U} over Ω_{ij} can be written in the form

$$R_h \mathbf{U} = \mathbf{U}_{ij} + (\mathbf{U}_x)_{ij}(x - x_i) + (\mathbf{U}_y)_{ij}(y - y_j) + (\mathbf{U}_{xy})_{ij}(x - x_i)(y - y_j), \quad (4.11)$$

where the slopes $(\mathbf{U}_x)_{ij}$, $(\mathbf{U}_y)_{ij}$, $(\mathbf{U}_{xy})_{ij}$ are, for example, second-order central difference approximations, as in (3.8).

Another choice (see also Noelle [27]) is to take some solution adaptive approximation of the exact derivatives, s.t. We have, for example, for an x -slope

$$(\mathbf{U}_x)_{ij} = \mathbf{u}_x(x_i, y_j) + (\hat{\mathbf{u}}_x)_{ij}h + \mathcal{O}(h^2), \quad (4.12)$$

where $(\hat{\mathbf{u}}_x)_{ij}$ is some discretely Lipschitz-continuous grid function. This means that there exists a constant $L > 0$ such that for any $i, j \in \mathbb{Z}$,

$$|(\hat{\mathbf{u}}_x)_{ij} - (\hat{\mathbf{u}}_x)_{i+1j}| \leq Lh.$$

A similar relationship holds for the y direction. It was shown in [12] that, for example, the central version of the WENO recovery (3.13) satisfies the above condition (4.12).

Let Q be the L^2 -projection given by integral averages onto a space S_h^0 of piecewise constant step functions,

$$Q\mathbf{u} = \sum_{i,j \in \mathbb{Z}} \left(\frac{1}{h^2} \int_{\Omega_{ij}} \mathbf{u}(x, y) dx dy \right) \chi_{ij}, \quad \mathbf{u} \in (L^2(\mathbb{R}^2))^m, \quad (4.13)$$

where χ_{ij} is the characteristic function for the square mesh cell Ω_{ij} . Denote by $\|\cdot\|$ the L^2 -norm. The global error between the exact solution \mathbf{u} and the approximate solution \mathbf{U} is then defined as

$$\mathbf{e}^{n+1} := \mathbf{u}(\cdot, t_{n+1}) - R_h \mathbf{U}^{n+1}.$$

The error can be decomposed into a recovered projection error $\boldsymbol{\eta}$ and an evolutionary error $\boldsymbol{\xi}$:

$$\mathbf{e}^{n+1} = (\mathbf{u}(t_{n+1}) - R_h Q\mathbf{u}(t_{n+1})) + (R_h Q\mathbf{u}(t_{n+1}) - R_h \mathbf{U}^{n+1}) \equiv \boldsymbol{\eta}^{n+1} + \boldsymbol{\xi}^{n+1}. \quad (4.14)$$

It is clear (see also [17]) that the projection error onto piecewise bilinear functions is of second order; i.e., $\|\boldsymbol{\eta}^{n+1}\| \leq ch^2$. Now we derive an evolution equation for $\boldsymbol{\xi}$ by introducing the term $R_h \mathcal{N}_h R_h Q\mathbf{u}$ as follows:

$$\boldsymbol{\xi}^{n+1} = R_h(Q\mathbf{u}(t_{n+1}) - \mathcal{N}_h R_h Q\mathbf{u}(t_n)) + (R_h \mathcal{N}_h R_h Q\mathbf{u}(t_n) - R_h \mathcal{N}_h R_h \mathbf{U}^n). \quad (4.15)$$

Note that the operator \mathcal{N}_h consists of three steps: linearization on each cell interface; evolution of the solution to the linearized, constant coefficient, hyperbolic system on each cell interface; and the finite volume update. We studied in [17, 22] stability of \mathcal{N}_h if applied to a constant coefficient system. Here, we assume that the linearization is chosen in such a way that the stability of the resulting scheme is preserved. Thus, we assume that the operator $R_h \mathcal{N}_h$ is strongly stable in a suitable norm, e.g., such as possibly the L^2 -norm

$$\|R_h \mathcal{N}_h\| \leq 1 \quad (4.16)$$

(see Remark 4.3). Then the last term is bounded by $\|\boldsymbol{\xi}^n\|$, so the evolutionary error $\boldsymbol{\xi}^{n+1}$ is in fact determined only by the recovered truncation error,

$$\mathbf{T}^n := \frac{1}{\Delta t} [Q\mathbf{u}(t_{n+1}) - \mathcal{N}_h R_h Q\mathbf{u}(t_n)], \quad (4.17)$$

through the recurrence relation $\|\boldsymbol{\xi}^{n+1}\| \leq \|\boldsymbol{\xi}^n\| + \Delta t \|R_h \mathbf{T}^n\|$. This yields

$$\|\boldsymbol{\xi}^{n+1}\| \leq \|\boldsymbol{\xi}^0\| + \Delta t \sum_{j=0}^n \|R_h \mathbf{T}^j\|.$$

Since the initial approximation is taken by

$$\mathbf{U}^0 := \frac{1}{h^2} \int_{\Omega_{ij}} \mathbf{u}(x, y, 0) dx dy,$$

we get $\boldsymbol{\xi}^0 = 0$, and it remains to prove the order of the truncation error.

Remark 4.3. Note that condition (4.16) is still an open problem for multidimensional nonlinear systems. It is only expected to hold under some CFL stability condition on $\Delta t/h$. Such a result has been established for some constant coefficient systems. It remains to be seen whether such a condition can be established for our operator \mathcal{N}_h , which includes a linearization, in the future.

In our previous paper [17], we proved that for the wave equation system the EG1, EG2, and EG3 approximate operators are stable if $\nu \equiv c\Delta t/h \leq \text{CFL} < 1$, for some $\text{CFL} \in]0, 1[$. In [20] precise CFL numbers for several EG schemes are computed experimentally. For example, the first-order EG1, EG2, and EG3 schemes are stable up to CFL numbers 0.78, 0.53, and 0.59, respectively. In our forthcoming paper [22], we study the stability question more closely and derive a new approximate EG operator which yields a FVEG scheme stable up to a natural stability limit $\text{CFL} = 1$. The whole derivation and theoretical as well as numerical justification is rather involved and is beyond the framework of the present paper. But results presented here will naturally apply also to this new EG operator.

4.3. Truncation Error Analysis

The aim of this subsection is to show the second-order truncation error estimates for the FVEG scheme applied to a constant coefficient linear hyperbolic system in two space dimensions. We have particularly in mind the linearized Euler equation system (2.2) and the wave equation system (2.5) with or without advection, i.e., systems with constant Jacobians. However, the general framework of the proof, except the part with the evolution operator, i.e., Lemma 4.5, which depends on the system under consideration, is the same for any linear, constant coefficient, hyperbolic system.

THEOREM 4.4. *Let \mathbf{v} be a smooth solution of the two-dimensional linearized, constant coefficient, Euler equation system (2.2), or of the wave equation system (2.5) (with or without advection). The truncation error \mathbf{T}^n of the FVEG scheme (3.5), (3.7) is of second order; i.e., for $\Delta t/h = \lambda$ fixed,*

$$\|\mathbf{T}^n\| = O(h^2).$$

Proof. We evaluate and compare both terms of \mathbf{T}^n in (4.17). For any $\mathbf{x} \in \Omega_{ij}$, $i, j \in \mathbb{Z}$, we have by Taylor expansion in time that

$$\mathbf{v}(\mathbf{x}, t_{n+1}) = \mathbf{v}(\mathbf{x}, t_n) + \Delta t \mathbf{v}_t(\mathbf{x}, t_n) + \frac{\Delta t^2}{2} \mathbf{v}_{tt}(\mathbf{x}, t_n) + \mathcal{O}(\Delta t^3). \quad (4.18)$$

Further, put

$$\mathbf{v}_{ij}^n := Q\mathbf{v}(\cdot, t_n)|_{\Omega_{ij}} = \frac{1}{h^2} \int_{\Omega_{ij}} \mathbf{v}(\mathbf{x}) \, d\mathbf{x}.$$

Then integrating (4.18) over Ω_{ij} , using (2.2) or an analogous formulation for the wave equation system, and the Gauss theorem yield

$$\begin{aligned}
Q\mathbf{v}(\cdot, t_{n+1})|_{\Omega_{ij}} &= \mathbf{v}_{ij}^{n+1} \\
&= \mathbf{v}_{ij}^n - \frac{\Delta t}{h^2} \int_{\partial\Omega_{ij}} (\mathbf{A}_1 n_x + \mathbf{A}_2 n_y) \mathbf{v}^n - \frac{\Delta t^2}{2h^2} \int_{\partial\Omega_{ij}} \partial_t((\mathbf{A}_1 n_x + \mathbf{A}_2 n_y) \mathbf{v}^n) + \mathcal{O}(\Delta t^3) \\
&= \mathbf{v}_{ij}^n - \frac{\Delta t}{h} [\mathbf{A}_1(\mathbf{v})_{i+1/2,j}^n - \mathbf{A}_1(\mathbf{v})_{i-1/2,j}^n] - \frac{\Delta t}{h} [\mathbf{A}_2(\mathbf{v})_{i,j+1/2}^n - \mathbf{A}_2(\mathbf{v})_{i,j-1/2}^n] \\
&\quad - \frac{\Delta t^2}{2h} [\mathbf{A}_1 \partial_t(\mathbf{v})_{i+1/2,j}^n - \mathbf{A}_1 \partial_t(\mathbf{v})_{i-1/2,j}^n] \\
&\quad - \frac{\Delta t^2}{2h} [\mathbf{A}_2 \partial_t(\mathbf{v})_{i,j+1/2}^n - \mathbf{A}_2 \partial_t(\mathbf{v})_{i,j-1/2}^n] + \mathcal{O}(h^3 + \Delta t^3), \tag{4.19}
\end{aligned}$$

where \mathbf{A}_k are the constant Jacobians of the fluxes $\mathbf{f}_k(\mathbf{v}) = \mathbf{A}_k \mathbf{v}$, $k = 1, 2$, and $\mathbf{n} = (n_x, n_y)$ is the outer normal vector to $\partial\Omega_{ij}$.

Now, applying $\mathcal{N}_h R_h$ to the exact solution $Q\mathbf{v}^n$ we get

$$\mathcal{N}_h R_h Q\mathbf{v}^n = \mathbf{v}_{ij}^n - \frac{\Delta t}{h} \sum_{k=1}^2 \delta_{x_k} \mathbf{f}_k(\mathbf{v}^*), \tag{4.20}$$

where \mathbf{v}^* is computed on the cell interfaces of Ω_{ij} by means of any approximate evolution operator EG1, EG2, or EG3, denoted now by $E_{\Delta t/2}$. Thus, we have, for example, on the right-hand edge $\mathcal{E}_{i+1/2}$

$$\mathbf{v}_{i+1/2}^* = \frac{1}{h} \int_{\mathcal{E}_{i+1/2}} E_{\Delta t/2} R_h Q\mathbf{v}^n \, dS, \tag{4.21}$$

Analogously it holds for the edge $\mathcal{E}_{i-1/2}$ and for the horizontal edges $\mathcal{E}_{j\pm 1/2}$.

In order to show the second-order estimates of the truncation error it is sufficient to prove that

$$\begin{aligned}
\mathbf{f}_1(\mathbf{v}_{i+1/2}^*) - \mathbf{f}_1(\mathbf{v}_{i-1/2}^*) &= [\mathbf{A}_1(\mathbf{v})_{i+1/2,j}^n - \mathbf{A}_1(\mathbf{v})_{i-1/2,j}^n] \\
&\quad + \frac{\Delta t}{2} [\mathbf{A}_1 \partial_t(\mathbf{v})_{i+1/2,j}^n - \mathbf{A}_1 \partial_t(\mathbf{v})_{i-1/2,j}^n] + \mathcal{O}(h^3), \tag{4.22}
\end{aligned}$$

together with the analogous equation for the horizontal fluxes.

But we have for each approximate evolution operator, i.e., the EG1, EG2, and EG3, the following Lemma. The proof will be postponed until later.

LEMMA 4.5. *Let R_h be a bilinear recovery such that slopes are approximated with an error $\mathcal{O}(h^2)$, e.g., by central differences (cf. (4.11)). Let $E_{\Delta t/2}$ be one of the evolution operators EG1, EG2, or EG3, derived in Section 2.2. Then the error between the exact solution $\mathbf{v}_{i\pm 1/2,j}^{n+1/2}$ at the midpoints of cell interfaces $\mathcal{E}_{i\pm 1/2}$ and the approximation $\mathbf{v}_{i\pm 1/2}^*$, obtained by the evolution Galerkin step (4.21), is of second order. More precisely, we have for the vertical cell interfaces*

$$\mathbf{v}_{i\pm 1/2}^* - (\mathbf{v})_{i\pm 1/2,j}^{n+1/2} = h^2 \mathbf{g}_{i\pm 1/2} + \mathcal{O}(h^3), \tag{4.23}$$

where the vector functions $\mathbf{g}_{i\pm 1/2}$ are discretely Lipschitz-continuous grid functions. An analogous error estimate holds for the horizontal cell interfaces.

Now we can rewrite the L.H.S. of (4.22) equivalently in the following way:

$$\begin{aligned}
 \mathbf{f}_1(\mathbf{v}_{i+1/2}^*) - \mathbf{f}_1(\mathbf{v}_{i-1/2}^*) &= \mathbf{A}_1(\mathbf{v}^*)_{i+1/2} - \mathbf{A}_1(\mathbf{v}^*)_{i-1/2} \\
 &= \mathbf{A}_1(\mathbf{v})_{i+1/2,j}^{n+1/2} - \mathbf{A}_1(\mathbf{v})_{i-1/2,j}^{n+1/2} + \mathcal{O}(h^3) \\
 &= \mathbf{A}_1 \left(\mathbf{v} + \frac{\Delta t}{2} \partial_t \mathbf{v} + \frac{\Delta t^2}{8} \partial_t^2 \mathbf{v} \right)_{i+1/2,j}^n \\
 &\quad - \mathbf{A}_1 \left(\mathbf{v} + \frac{\Delta t}{2} \partial_t \mathbf{v} + \frac{\Delta t^2}{8} \partial_t^2 \mathbf{v} \right)_{i-1/2,j}^n + \mathcal{O}(h^3 + \Delta t^3). \tag{4.24}
 \end{aligned}$$

Subtracting (4.24) from the R.H.S. of (4.22) we get a rest term \mathbf{r}_{ij}^n , s.t.,

$$\mathbf{r}_{ij}^n := \Delta t^2/8 \mathbf{A}_1 \left((\partial_t^2 \mathbf{v})_{i+1/2,j}^n - (\partial_t^2 \mathbf{v})_{i-1/2,j}^n \right) + \mathcal{O}(h^3 + \Delta t^3). \tag{4.25}$$

However, the second derivatives of \mathbf{v} in \mathbf{r}_{ij} are discretely Lipschitz-continuous grid functions \mathbf{g} , and thus it holds that $\mathbf{g}_{i+1/2} - \mathbf{g}_{i-1/2} = \mathcal{O}(h)$. This implies that

$$\mathbf{r}_{ij}^n = \mathcal{O}(h^3). \tag{4.26}$$

Combining (4.25), (4.26) with (4.22), (4.24) yields

$$\|\mathbf{T}^n\| = \mathcal{O}(h^2),$$

which concludes the proof.

Remark 4.6. The same results can be shown also for the case of a bilinear recovery R_h ; s.t. (4.12) holds, e.g., the central version of WENO recovery. The first-order terms $(\hat{\mathbf{v}}_x)_{ij}h$ in (4.12) are Lipschitz-continuous grid functions, and therefore they lead to the same order of error as the central differences, if the fluxes on cell interfaces are subtracted in (4.24).

Remark 4.7. Note that the proof above can be extended formally also to nonlinear systems with Jacobians \mathbf{A}_k frozen at time $\tilde{t} = t_n + \Delta t/2$; i.e., $\mathbf{A}_k(x, y) = \mathbf{A}_k(\mathbf{u}(x, y, \tilde{t}))$. One interesting example of this situation would be linearized, constant coefficient, system (2.2) rewritten in the conservative variables \mathbf{u} . As a result we get a system in conservative variables with nonconstant Jacobians. The proof above, more precisely the part concerning the finite volume update, can be easily extended to this case. We would need to assume again that the exact solution is smooth enough; i.e., for some final time $T > 0$, $\mathbf{u} \in C^2(\]0, T[)$, with spatially Lipschitz-continuous $\mathbf{u}_{t\tilde{t}}$. Moreover, we need to suppose that the conservative fluxes $\mathbf{f}_k(\mathbf{u}) \in C^2$, $k = 1, 2$, with Lipschitz-continuous second derivative. Note that only smooth solutions locally in time are considered, i.e., before shocks evolve. Now we proceed to prove Lemma 4.5.

Proof (Lemma 4.5). Consider the linear hyperbolic system of Euler equations (2.2) or the wave equation system (2.5). Thus, the Jacobian matrices \mathbf{A}_k , $k = 1, 2$, are constant. Denote by \mathbf{Id} the identity matrix and by \mathbf{D}_k the diagonal part of \mathbf{A}_k . For example, in the case of the Euler equations (2.2) or of the wave equation system with advection (2.5), \mathbf{D}_k is the advective part and we have $\mathbf{D}_1 = \tilde{u}\mathbf{Id}$, $\mathbf{D}_2 = \tilde{v}\mathbf{Id}$. Let $\mathbf{M}_k := \mathbf{A}_k - \mathbf{D}_k$, $k = 1, 2$, and denote by L the linear operator $\mathbf{M}_1 \partial_x + \mathbf{M}_2 \partial_y$. Then the linear hyperbolic systems, which

we consider, can be written in the following form:

$$\mathbf{v}_t + \mathbf{D}_1 \mathbf{v}_x + \mathbf{D}_2 \mathbf{v}_y \equiv \mathbf{v}_t + \tilde{u} \mathbf{v}_x + \tilde{v} \mathbf{v}_y = -L\mathbf{v}. \quad (4.27)$$

Define a directional derivative σ by

$$\frac{d}{d\sigma} := \frac{\partial}{\partial t} + \tilde{u} \frac{\partial}{\partial x} + \tilde{v} \frac{\partial}{\partial y}. \quad (4.28)$$

Now, we apply the Taylor expansion with respect to σ at the midpoint of $\mathcal{E}_{i+1/2}$ and use (4.27) to obtain

$$\mathbf{v}_{i+1/2,j}^{n+1/2} = \mathbf{v}_{P'} - \frac{\Delta t}{2} L \mathbf{v}_{P'} + \frac{\Delta t^2}{8} L^2 \mathbf{v}_{P'} + \mathcal{O}(\Delta t^3), \quad (4.29)$$

where $P' = (x_{i+1/2} - \tilde{u} \Delta t / 2, y_j - \tilde{v} \Delta t / 2, t^n)$.

On the other hand, we have from the evolution Galerkin step (4.21)

$$\mathbf{v}_{i+1/2}^* = \mathbf{v}_{P'} - \frac{\Delta t}{2} L_h \mathbf{v}_{P'} + \Delta t^2 M_h \mathbf{v}_{P'}, \quad (4.30)$$

where L_h, M_h are finite difference operators defined by the corresponding EG operator.

After some calculations, for each EG operator the properties

$$L_h = L + \mathcal{O}(h^2), \quad M_h = \alpha L^2 + \mathcal{O}(h^2), \quad (4.31)$$

where $\alpha \in \mathbb{R}^m$, can be shown. Here m is the number of equations of the hyperbolic system. Subtracting (4.30) from (4.29) and using (4.31) leads to (4.23) for the edge $\mathcal{E}_{i+1/2}$.

Let us illustrate the situation more precisely for the wave equation system, without advection, and consider only the 1D data case for simplicity of derivation. Then we have for the first component of the exact solution (ϕ, u)

$$\phi^{n+1/2} = \phi^n - \frac{c \Delta t}{2} u_x^n + \frac{c^2 \Delta t^2}{8} \phi_{xx}^n + \mathcal{O}(\Delta t^3). \quad (4.32)$$

Assume that the both Mach cone and cell interface integrals are computed exactly for discontinuous bilinear approximate functions given by (3.8). The EG3 approximate evolution operator (4.21) gives the following equation for the first component ϕ of the cell interface intermediate state (see also [19], where stencil coefficients are written explicitly):

$$\begin{aligned} \phi^* &= \left[1 + \left(\frac{\nu}{2\pi} - \frac{1}{4} \right) \delta_x^2 \right] \mu_x \phi^n - \left[\frac{\nu}{2} + \left(\frac{\nu}{8} - \frac{1}{2\pi} \right) \delta_x^2 \right] \delta_x u^n \\ &= \phi^n - \frac{c \Delta t}{2} u_x^n + \left(\frac{1}{4} + \frac{\nu}{2\pi} \right) h^2 \phi_{xx}^n - \left(\frac{\nu}{24} + \frac{1}{2\pi} \right) h^3 u_{xxx}^n + \mathcal{O}(h^4). \end{aligned} \quad (4.33)$$

We remind readers that $\nu = c \Delta t / h$ defines a CFL number for the wave equation system. Thus, subtracting (4.32) from (4.33) gives

$$\phi^* - \phi^{n+1/2} = \alpha h^2 \phi_{xx}^n + \mathcal{O}(h^3),$$

with $\alpha = (\nu/2\pi + 1/4 - \nu^2/8)$. An analogous property can be shown for the edge $\mathcal{E}_{i-1/2}$ and for the second variable u , as well as for the complete two-dimensional situation. Any second-order term consists of the second-order derivatives, which are Lipschitz-continuous grid functions. This concludes the proof.

COROLLARY 4.8. *The truncation error \mathbf{T}^n of the FVEG scheme (3.5), (3.6) is of first order; i.e., for $\Delta t/h = \lambda$ fixed,*

$$\|\mathbf{T}^n\| = O(h).$$

Proof. The crucial point is to show that if no recovery is used, we have for the evolution Galerkin step the first-order-error estimates

$$\mathbf{v}_{i+1/2}^* - (\mathbf{v})_{i+1/2,j}^{n+1} = h\mathbf{g}_{i+1/2} + O(h^2), \quad (4.34)$$

where the vector functions $\mathbf{g}_{i+1/2}$ are discretely Lipschitz-continuous grid functions. This can be verified, after some computation, for each of the EG operators in away analogous to that in Lemma 4.5. For example, for the 1D data case of the wave equation system, we have for the first component ϕ^*

$$\begin{aligned} \phi^* &= \mu_x \phi^n - \frac{2}{\pi} \delta_x u^n \\ &= \phi^n - \frac{2}{\pi} h u_x^n + \frac{h^2}{2} \phi_{xx}^n - \frac{2}{3\pi} h^3 u_{xxx}^n + O(h^4). \end{aligned} \quad (4.35)$$

Again, subtracting the equation for the exact solution (4.32) from (4.35) gives

$$\phi^* - \phi^{n+1/2} = \alpha h u_x^n + O(h^2),$$

with $\alpha = (\nu/2 - 2/\pi)$, which concludes the proof.

5. NUMERICAL EXPERIMENTS

In this section, through numerical experiments, we illustrate the performance of the proposed methods and compare it with other schemes. The computational domain was taken to be a square $[-1, 1] \times [-1, 1]$. The experiments were done on rectangular meshes with the FVEG3 scheme (cf. (2.17)–(2.20)) for the second-order method the minmod slope limiter (3.12) was used. We set the CFL number $\nu = \max(|u| + c, |v| + c)\Delta t/h$ to 0.55.

The first example is a two-dimensional Sod problem with the initial data

$$\begin{aligned} \rho &= 1, & u &= 0, & v &= 0, & p &= 1, & \|\mathbf{x}\| &< 0.4; \\ \rho &= 0.125, & u &= 0, & v &= 0, & p &= 0.1, & \text{else.} \end{aligned}$$

Since the mesh is quadrilateral, the initial data are implemented by cutting the initial discontinuity and assigning it by modified area-weighted values according to the corresponding cell. Figure 2 shows the isolines of density, the x - and y -velocity components, and the pressure computed at time $T = 0.2$ by the second-order FVEG3 scheme. The solution exhibits a circular shock traveling away from the center, a circular contact discontinuity traveling

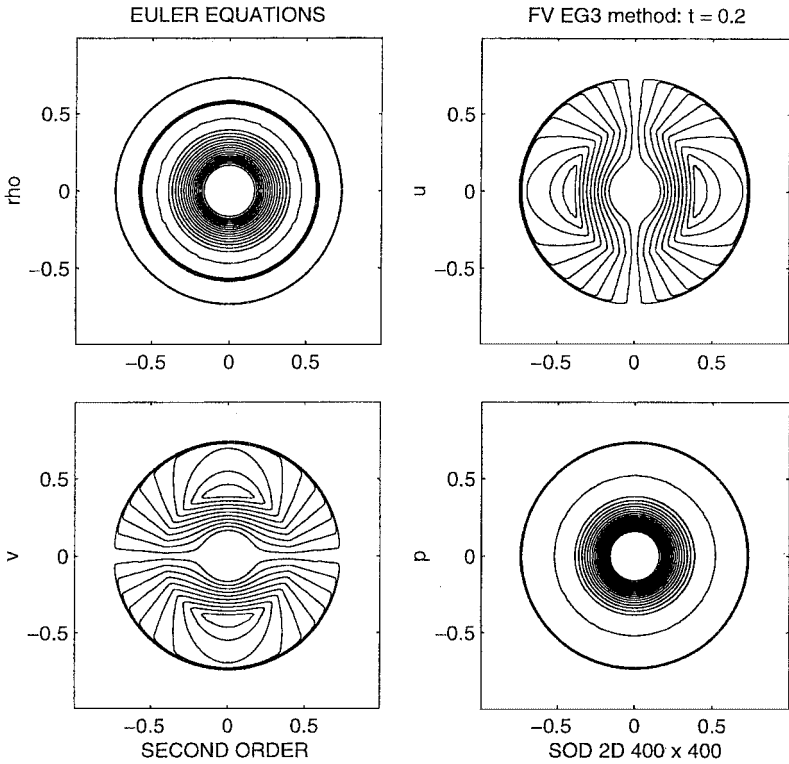


FIG. 2. Cylindrical explosion. Isolines of the solution obtained by the FVEG3 scheme with the Simpson rule at $T = 0.2$ on a 400×400 mesh.

in the same direction, and a circular rarefaction wave traveling toward the origin at $(0, 0)$. The cell interface integrals of fluxes are approximated with the Simpson rule. This result illustrates good multidimensional resolution and preservation of rotational symmetry of numerical solution. In Fig. 3 we show isolines of the solution computed by the second-order FVEG3 method, which uses the trapezoidal rule for the approximation of cell interface integrals. As we mentioned in Section 3.2, this quadrature yields a FV scheme which is not monotonic and has oscillations in the solution (see also [22] for more details).

In order to get more information on the exact solution, we solved on a very fine mesh the one-dimensional nonhomogeneous cylindrically symmetric Euler equations using the second-order finite volume method of Roe with the minmod slope limiter; i.e.,

$$\mathbf{U}_t + \mathbf{F}(\mathbf{U})_r = \mathbf{T}(\mathbf{U}), \quad (5.1)$$

with

$$\mathbf{U} := \begin{pmatrix} \rho \\ \rho \hat{u} \\ e \end{pmatrix}, \quad \mathbf{F}(\mathbf{U}) := \begin{pmatrix} \rho \hat{u} \\ \rho \hat{u}^2 + p \\ (e + p) \hat{u} \end{pmatrix}, \quad \mathbf{T}(\mathbf{U}) := -\frac{1}{r} \begin{pmatrix} \rho \hat{u} \\ \rho \hat{u}^2 \\ (e + p) \hat{u} \end{pmatrix}.$$

Here, r is the radial direction and \hat{u} is the radial velocity. Figure 4 shows the comparison between the “exact” solution obtained by the one-dimensional FVM and the numerical

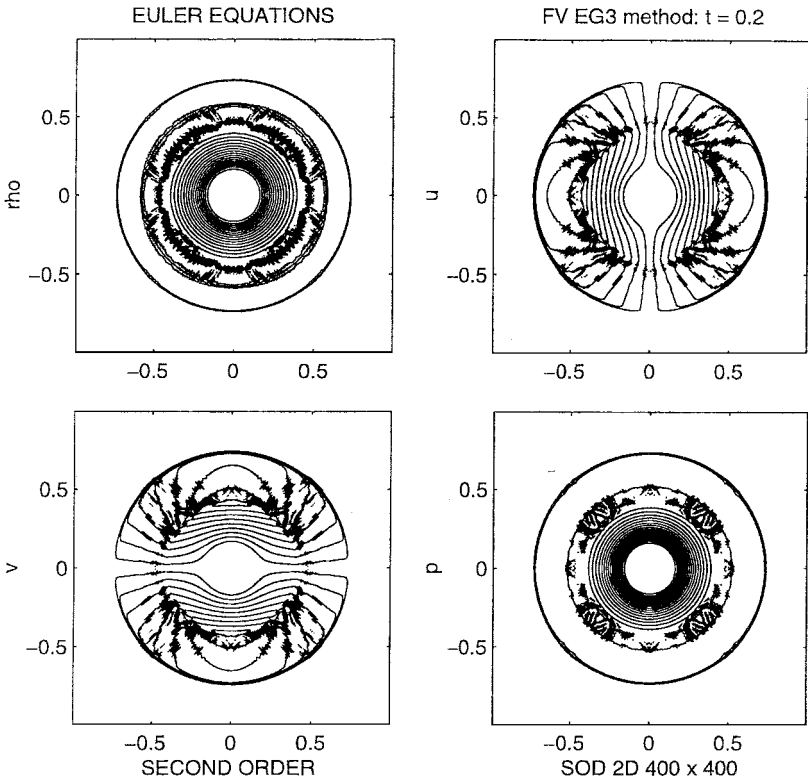


FIG. 3. Same as Fig. 2, but using the trapezoidal instead of Simpson's rule.

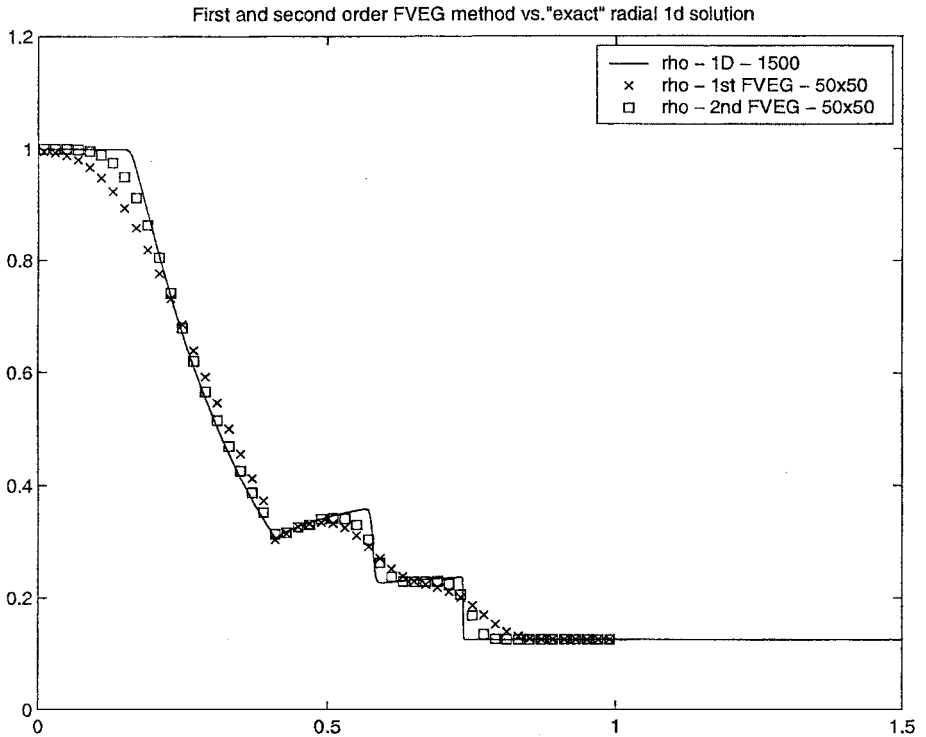


FIG. 4. Comparison between the one-dimensional cylindrically symmetric solution and the first- and second-order FVEG methods.

solution obtained by the first- as well as the second-order FVEG3 methods at the $y = 0$ cross section. In the first-order method, integrals along cell interfaces are evaluated exactly. For the second-order method the Simpson rule approximation was used. The Mach cone integrals from 0 to 2π appearing in the approximate evolution operator are evaluated exactly. We can notice that the second-order method resolves discontinuities more sharply and approximates the maxima of the solution more accurately. Note that we do not need any artificial entropy fix in order to resolve correctly the sonic rarefaction wave. This is done automatically by the method.

The second example is a two-dimensional Riemann problem. The computational domain $[-1, 1] \times [-1, 1]$ is divided into four quadrants. The initial data consist of single constant states in each of the four quadrants. These constants are chosen so that each pair of quadrants define a one-dimensional Riemann problem producing a single wave, which could be a shock, rarefaction, or slip contact discontinuity. The aim is to study interactions of these elementary waves. This problem was studied by Schulz-Rinne *et al.* [31] for several initial configurations. Afterward, many authors compared the performance of their multidimensional solvers on this “benchmark” problem (see, e.g., Brio *et al.* [3], Fey [9], LeVeque [13], Liska and Wendroff [16]).

First let us consider the following initial data:

$$\begin{array}{llll} \rho = 0.5313, & u = 0.0, & v = 0.0, & p = 0.4, \quad \text{if } x > 0, \quad y > 0; \\ \rho = 1.0, & u = 0.0, & v = 0.7276, & p = 1.0, \quad \text{if } x > 0, \quad y < 0; \\ \rho = 1.0, & u = 0.7276, & v = 0.0, & p = 1.0, \quad \text{if } x < 0, \quad y > 0; \\ \rho = 0.8, & u = 0.0, & v = 0.0, & p = 1.0, \quad \text{if } x < 0, \quad y < 0. \end{array}$$

For this configuration two forward-moving shocks and two standing slip lines are produced. The solution contains a Mach reflection shown in Fig. 5 for density isolines. It was reported by Fey in [8] that classical directional splitting FV schemes, e.g., the Van Leer flux vector splitting method, may produce a curved shock connected with two other shocks, resembling

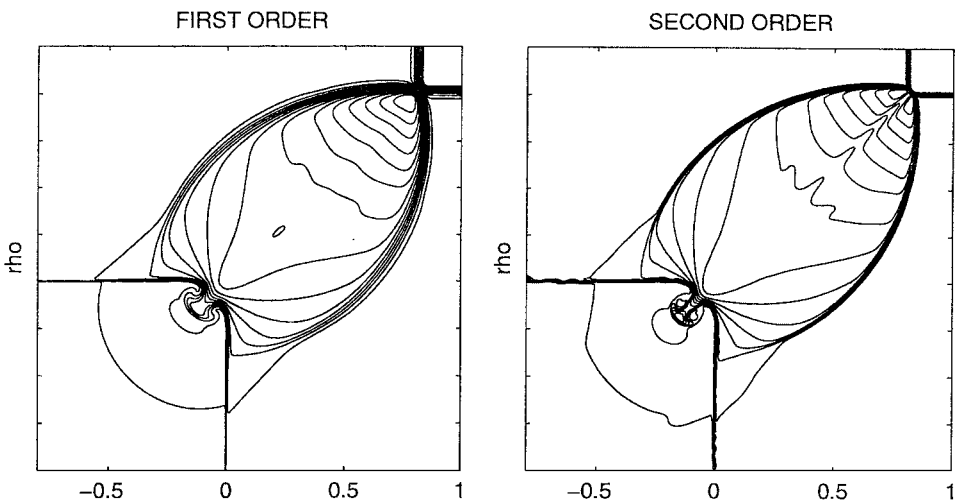


FIG. 5. Riemann problem with two shocks/two slip lines. Isolines of the density obtained by the (left) first- and (right) second-order FVEG3 schemes at $T = 0.52$ on a 400×400 mesh.

regular shock reflection. Fey's method of transport [8] resolves the solution correctly as a Mach reflection. Figure 5 demonstrates that the second-order FVEG3 method resolves the multidimensional features in the $x = y$ direction correctly. For a comparison we have plotted also the solution obtained by the first-order FVEG3 method. Notice that due to the numerical dissipation the Mach reflection is smoothed.

The third example is a two-dimensional Riemann problem that produces two forward-moving shocks and two backward-moving shocks. The initial data is given by

$$\begin{aligned} \rho &= 1.1, & u &= 0.0, & v &= 0.0, & p &= 1.1, & \text{if } x > 0, & y > 0; \\ \rho &= 0.5065, & u &= 0.0, & v &= 0.8939, & p &= 0.35, & \text{if } x > 0, & y < 0; \\ \rho &= 0.5065, & u &= 0.8939, & v &= 0.0, & p &= 0.35, & \text{if } x < 0, & y > 0; \\ \rho &= 1.1, & u &= 0.8939, & v &= 0.8939, & p &= 1.1, & \text{if } x < 0, & y < 0. \end{aligned}$$

In Fig. 6 isolines of solution obtained by the second-order FVEG3 method are plotted. The Mach reflection in $x = -y$ is well resolved (see isolines of density and velocity components). Computational costs of the FVEG3 schemes are in general comparable with other well-known first- and second-order FV methods. In [32] implementations of different boundary conditions for the FVEG schemes are studied.

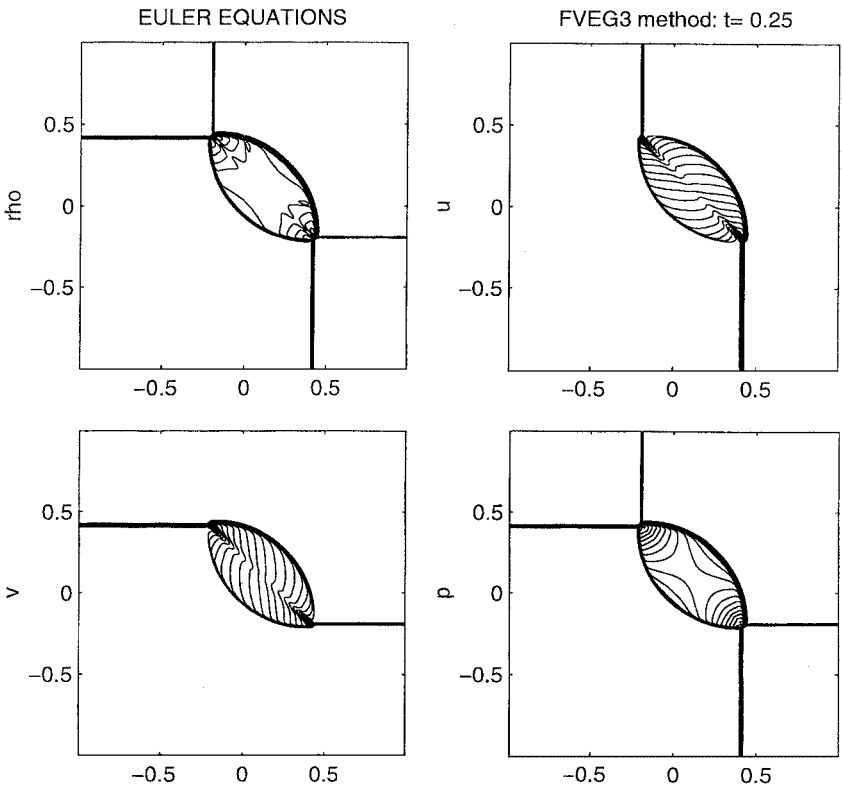


FIG. 6. Riemann problem with four shocks. Isolines of the solution obtained by the second-order FVEG3 scheme at $T = 0.25$ on a 400×400 mesh.

6. CONCLUSION

In this paper we have derived new FVEG schemes for nonlinear Euler equations of gas dynamics. The methods consist of two steps and couple a finite volume formulation with the approximate evolution Galerkin operator. The latter is constructed using the bicharacteristics of the multidimensional hyperbolic system such that all of the infinitely many directions of wave propagation are taken into account. In Section 2.2 we have derived three approximate EG operators for the Euler equations. In the first step of the FVEG method the solution at cell interfaces is evolved by the approximate evolution operator and fluxes along edges are calculated. In the second step the finite volume update is done. The second-order FVEG scheme works with a conservative piecewise bilinear recovery in space and the midpoint rule approximation of the time integral. We analyze the linearization error in time and derive the estimates for the global error in time as well as in space under the assumption that the linearization in space preserves stability of the numerical scheme. Further, the truncation error is analyzed for the linear wave equation system and the linearized, constant coefficient, Euler equations. It is shown that the error of the FVEG scheme (3.5), (3.7) applied to the wave equation system or linear, constant coefficient, Euler equations is of second order. Numerical experiments confirm good multidimensional behavior and higher order resolution for the second-order FVEG methods.

In this paper we have described the FVEG schemes using regular square mesh cells. Generalization to arbitrary meshes is only a matter of the implementation and will be done in future. In our forthcoming paper [22] we will study the question of stability more closely and derive a new EG operator which yields for the FVEG method the CFL limit 1.

ACKNOWLEDGMENTS

This research was supported under DFG Grant Wa 633/6-2 of the Deutsche Forschungsgemeinschaft, the VolkswagenStiftung grant agency, and partially by Grants GACR 201/00/0557 and CZ 39001/2201 of the Czech Grant Agency. The authors thank K.W. Morton (Oxford/Bath Universities) for stimulating discussions on the topic.

REFERENCES

1. T. J. Barth and D. C. Jespersen, *The Design and Application of Upwind Schemes on Unstructured Meshes*, AIAA paper 336 (1989).
2. S. Billet and E. F. Toro, On WAF-type schemes for multidimensional hyperbolic conservation laws, *J. Comput. Phys.* **130**, 1 (1997).
3. M. Brio, A. R. Zakharian, and G. M. Webb, Two-dimensional Riemann solver for Euler equations of gas dynamics, *J. Comput. Phys.*, in press.
4. D. S. Butler, The numerical solution of hyperbolic systems of partial differential equations in three independent variables, *Proc. R. Soc. London* **255A**, 233 (1960).
5. P. N. Childs, *The Characteristic Galerkin Method for Hyperbolic Conservation Laws*, Ph.D. thesis (Oxford University, 1988).
6. P. Collela, Multidimensional upwind methods for hyperbolic conservation laws, *J. Comput. Phys.* **87**, 171 (1990).
7. H. Deconinck, P. Roe, and R. Struijs, A multidimensional generalization of Roe's flux difference splitter for the Euler equations, *Comput. Fluids* **22**(2-3), 215 (1993).
8. M. Fey, Multidimensional upwinding. Part I. The method of transport for solving the Euler equations, *J. Comput. Phys.* **143**, 159 (1998).

9. M. Fey, Multidimensional upwinding. Part II. Decomposition of the Euler equations into advection equations, *J. Comput. Phys.* **143**, 181 (1998).
10. H. Gilquin, J. Laurens, and C. Rosier, Multi-dimensional Riemann problems for linear hyperbolic systems, *M² AN* **30**(5), 527 (1996).
11. E. Isaacson and H. B. Keller, *Analysis of Numerical Methods* (Wiley, New York, 1966).
12. G.-S. Jiang and C.-W. Shu, Efficient implementation of weighted ENO schemes, *J. Comput. Phys.* **126**, 201 (1996).
13. R. J. LeVeque, Wave propagation algorithms for multi-dimensional hyperbolic systems, *J. Comput. Phys.* **131**, 327 (1997).
14. J. Li, T. Zhang, and S. Yang, *The Two-Dimensional Riemann Problem in Gas Dynamics*, Pitman Monographs and Surveys in Pure and Applied Mathematics 98 (Longman, 1998).
15. P. Lin, K. W. Morton, and E. Süli, Characteristic Galerkin schemes for scalar conservation laws in two and three space dimensions, *SIAM J. Numer. Anal.* **34**(2), 779 (1997).
16. R. Liska and B. Wendroff, Composite centered schemes for multidimensional conservation laws, *Int. Ser. Numer. Math.* **130**, 661 (1999).
17. M. Lukáčová-Medvid'ová, K. W. Morton, and G. Warnecke, Evolution Galerkin methods for hyperbolic systems in two space dimensions, *Math. Comp.* **69**, 1355 (2000).
18. M. Lukáčová-Medvid'ová, K. W. Morton, and G. Warnecke, Finite volume evolution Galerkin methods for multidimensional hyperbolic problems, in *Proceedings of the Finite Volumes for Complex Applications*, edited by R. Vilsmeier *et al.* (Hermès, 1999), p. 289.
19. M. Lukáčová-Medvid'ová, K. W. Morton, and G. Warnecke, High-resolution finite volume evolution Galerkin schemes for multidimensional conservation laws, in *Proceedings of ENUMATH'99* (World Scientific, Singapore, 1999), p. 0.
20. M. Lukáčová-Medvid'ová, K. W. Morton, and G. Warnecke, On high-resolution finite volume evolution Galerkin schemes for genuinely multidimensional hyperbolic conservation laws, in *Proceedings of the European Congress on Computational Methods in Applied Sciences and Engineering, ECCOMAS 2000, Barcelona, Spain*.
21. M. Lukáčová-Medvid'ová, K. W. Morton, and G. Warnecke, Finite volume evolution Galerkin methods for Euler equations of gas dynamics, *Int. J. Numer. Methods Fluids*, in press.
22. M. Lukáčová-Medvid'ová, K. W. Morton, and G. Warnecke, Finite volume evolution Galerkin (FVEG) methods for hyperbolic problems, manuscript in preparation.
23. M. Lukáčová-Medvid'ová and G. Warnecke, Lax-Wendroff type second order evolution Galerkin methods for multidimensional hyperbolic systems, *East-West J.* **8**(2), 127 (2000).
24. M. Lukáčová-Medvid'ová, G. Warnecke, and Y. Zahaykah, Evolution Galerkin methods for the multi-dimensional wave equation system, in *Proceedings of the International Symposium on Electromagnetic Compatibility, Magdeburg, Germany, 67–72, 1999*.
25. K. W. Morton, On the analysis of finite volume methods for evolutionary problems, *SIAM J. Numer. Anal.* **35**(6), 2195 (1998).
26. K. W. Morton and P. Roe, Vorticity-preserving Lax-Wendroff-type schemes for the system of wave equation, *SIAM J. Sci. Comput.* **23**(1), 170 (2001).
27. S. Noelle, The MOT-ICE: a new high-resolution wave-propagation algorithm for multi-dimensional systems of conservative laws based on Fey's method of transport, *J. Comput. Phys.* **164**, 283 (2000).
28. S. Ostkamp, Multidimensional characteristic Galerkin schemes and evolution operators for hyperbolic systems, *Math. Methods Appl. Sci.* **20**, 1111 (1997).
29. J. Quirk, A contribution to the great Riemann solver debate, *Int. J. Numer. Methods Fluid Dyn.* **18**, 555 (1994).
30. P. Roe, Discrete models for the numerical analysis of time-dependent multidimensional gas dynamics, *J. Comput. Phys.* **63**, 458 (1986).
31. C. W. Schulz-Rinne, J. P. Colins, and H. M. Glaz, Numerical solution of the Riemann problem for two-dimensional gas dynamics, *SIAM J. Sci. Comput.* **14**, 1394 (1993).
32. Y. Zahaykah, *Evolution Galerkin Schemes and Discrete Boundary Conditions for Multidimensional First Order Systems*, Ph.D. thesis (University of Magdeburg, 2002).